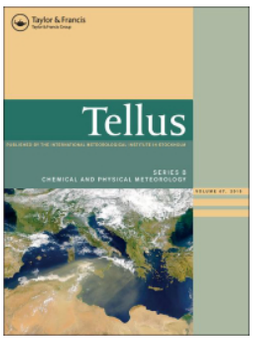

Tellus B: Chemical and Physical Meteorology

ISSN: (Print) 1600-0889 (Online) Journal homepage: https://www.tandfonline.com/loi/zelb20

# Can bottom-up ocean $CO_2$ fluxes be reconciled with atmospheric $^{13}C$ observations?

Caroline Alden, John Miller & James White

**To cite this article:** Caroline Alden, John Miller & James White (2010) Can bottom-up ocean $CO_2$ fluxes be reconciled with atmospheric $^{13}C$ observations?, Tellus B: Chemical and Physical Meteorology, 62:5, 369-388, DOI: 10.1111/j.1600-0889.2010.00481.x

**To link to this article:** https://doi.org/10.1111/j.1600-0889.2010.00481.x

Tellus SERIES B CHEMICAL AND PHYSICAL METEOROLOGY
PUBLISHED BY THE INTERNATIONAL METEOROLOGICAL INSTITUTE IN STOCKHOLM

*Tellus (2010), 62B, 369–388*



TELLUS

# Can bottom-up ocean $CO_2$ fluxes be reconciled with atmospheric $^{13}C$ observations?

*By* CAROLINE B. ALDEN[1], JOHN B. MILLER[2,3,*] and JAMES W.C. WHITE[1] [1]*Institute of Arctic and Alpine Research, University of Colorado, Boulder, CO 80309, USA*; [2]*National Oceanic & Atmospheric Administration Earth Systems Research Laboratory (NOAA/ESRL), 325 Broadway, Boulder, CO 80305, USA*; [3]*Cooperative Institute for Research in Environmental Sciences (CIRES), University of Colorado, Boulder, CO 80309, USA*

(Manuscript received 1 January 2010; in final form 18 June 2010)

ABSTRACT

The rare stable carbon isotope, $^{13}C$, has been used previously to partition $CO_2$ fluxes into land and ocean components. Net ocean and land fluxes impose distinctive and predictable fractionation patterns upon the stable isotope ratio, making it an excellent tool for distinguishing between them. Historically, isotope constrained inverse methods for calculating $CO_2$ surface fluxes—the 'double deconvolution'—have disagreed with bottom-up ocean flux estimates. In this study, we use the double deconvolution framework, but add, as a constraint, independent estimates of time histories of ocean fluxes to the atmospheric observations of $CO_2$ and $^{13}CO_2$. We calculate timeseries of net land flux, total disequilibrium flux and terrestrial disequilibrium flux from 1991 to 2008 that are consistent with bottom-up net ocean fluxes. We investigate possible drivers of interannual variability in terrestrial disequilibrium flux, including terrestrial discrimination, and test the sensitivity of our results to those mechanisms. We find that $C_3$ plant discrimination and shifts in the global composition of $C_3$ and $C_4$ vegetation are likely drivers of interannual variability in terrestrial disequilibrium flux, while contributions from heterotrophic respiration and disturbance anomalies are also possible.

## 1. Introduction

The atmospheric growth rate of $CO_2$ and global fossil fuel emissions are both well known, with low uncertainty. This means that the calculated net surface exchange history, the combined ocean and terrestrial biospheric fluxes, is also well known. The partitioning of these sinks into oceanic and biospheric components is less certain, however, as are the relative influences of the different mechanisms controlling the rate of change of atmospheric $CO_2$, which varied interannually by 0.55 ppm $yr^{-1}$ from 1979 to 2008 ($1\sigma$ standard deviation; Fig. 1) (Defries et al., 2002; Houghton, 2003; Matsumoto et al., 2004; van der Werf et al., 2004; Denman et al., 2007; Le Quéré et al., 2009). Elucidating the drivers of this variability is crucial for future projections of the magnitude of the airborne fraction, which is the proportion of fossil fuel emissions remaining in the atmosphere given net $CO_2$ exchange with the oceans and terrestrial biosphere. With greenhouse gas forced climate change happening, we must garner all of the tools that we have available to understand the controls on the variability of carbon exchange at the earth's surface.

There are two basic and complementary approaches to estimating surface fluxes of carbon. One is the 'top-down' method in which atmospheric observations are used to calculate surface exchanges. In this method, $CO_2$ concentrations can be augmented with isotopic data and other species, such as $O_2$ concentrations (e.g. Battle et al., 2000; Bender et al., 2005), to better constrain what is happening at the surface. The other, or 'bottom-up' method, is to measure or model surface fluxes directly. The primary weakness in the top-down method is a lack of specificity in the processes acting at the surface; this method can tell that a flux is occurring, for example, but is less informative about what causes that flux or how it may vary over time. The bottom-up approach is more directly informative about processes, but its primary weakness is the scaling problem it entails; surface observations are often limited in space and time and thus scaling up from local observations to regional to global fluxes is a challenge. Bottom-up models do not suffer from scaling issues, but are uncertain due to imperfect parameterization of processes. Bottom-up and top-down approaches are naturally complementary, and each provides a valuable check on the other.

$\delta^{13}C$ of $CO_2$ has been used numerous times for partitioning ocean and land flux magnitudes from an atmospheric, or top-down, perspective, primarily because fractionation against the heavier $^{13}C$ isotope is strong (about $-16‰$ globally) during

*Corresponding author.
e-mail: john.b.miller@noaa.gov
DOI: 10.1111/j.1600-0889.2010.00481.x

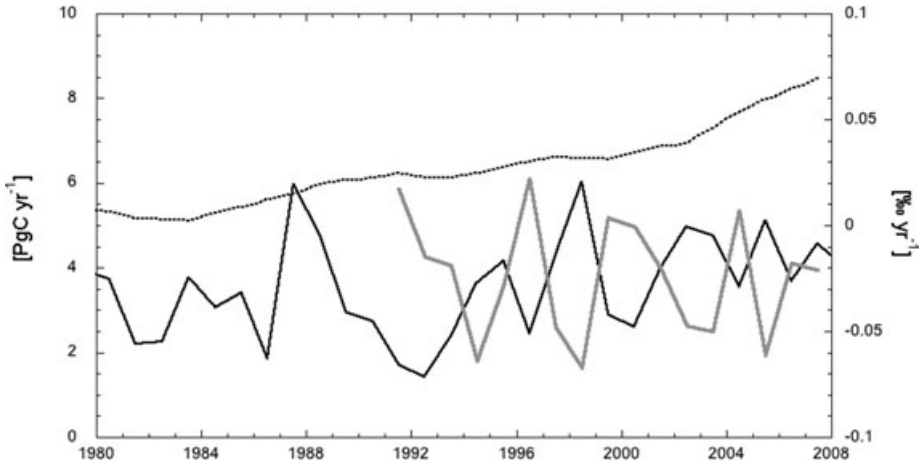


*Fig. 1.* Atmospheric $\delta^{13}CO_2$ growth rate (grey line), atmospheric $CO_2$ growth rate (solid black line) and $CO_2$ emissions from fossil fuel combustion and cement production (dotted black line); global annual means.

photosynthesis, but is only about $-2‰$ during ocean uptake of $CO_2$ (Francey, 1985; Farquhar et al., 1989; Keeling et al., 1989; Ciais et al., 1995; Enting et al., 1995; Zhang et al., 1995; Battle et al., 2000; Rayner et al., 2008). The double deconvolution approach is the traditional $\delta^{13}C$ budgeting technique (Keeling et al., 1989; Ciais et al., 1995), so-called because it solves two equations (eqs. 1 and 2) for the net terrestrial and oceanic surface $CO_2$ fluxes simultaneously. A major problem with the double deconvolution is that it is difficult to accurately model or measure a key term in the $^{13}C$ atmospheric budget, the disequilibrium flux (eqs. 4a and b). Because the burning of fossil fuels depletes atmospheric $\delta^{13}C$ (depletion averaged $-0.024‰$ yr$^{-1}$ between 1991 and 2008), the gross $CO_2$ fluxes into and out of land and ocean reservoirs are in isotopic disequilibrium. The release to the atmosphere of carbon with an isotopic signature reflective of uptake from an older, more enriched atmosphere results in a disequilibrium flux, which is expressed here in units of PgC‰ yr$^{-1}$. Disequilibrium flux and disequilibrium, or the isodisequilibrium forcing coefficient, are defined in Section 2.3.

As others have found and we will show, the double deconvolution approach results in interannual variability in the global net air–sea $CO_2$ flux that is much greater than bottom-up estimates from ocean model simulations and empirical data (Joos and Bruno, 1998; Lee et al., 1998; Le Quéré et al., 2003). Many recent modelling and observation studies reinforce the long-standing bottom-up perspective that interannual variability in ocean–atmosphere $CO_2$ fluxes is low when compared to most top-down approaches (Winguth et al., 1994). For example, Le Quéré et al. (2003) found that modelled $CO_2$ fluxes varied interannually by just $\pm 0.35$ PgC yr$^{-1}$ from 1980 to 2000. In the same study, they found that interannual variability in ocean $CO_2$ fluxes was only slightly higher when calculated by inversion of atmospheric $CO_2$ measurements using a three-dimensional atmospheric transport model, and by a multitracer inversion with $O_2/N_2$ and $\delta^{13}C$ measurements, but that double deconvolution flux variability was $\pm 1.4$ PgC yr$^{-1}$ (Le Quéré et al., 2003). Lee et al. (1998) calculated oceanic $CO_2$ uptake with a $1\sigma$ standard deviation of 0.2 PgC yr$^{-1}$ for 1982–1995, using $pCO_2$ climatology. Examination of Fig. 4 in that paper shows mean interannual flux anomalies of roughly $\pm 0.1$ PgC yr$^{-1}$ (Lee et al., 1998). The ecosystem–biogeochemistry model of Doney et al. (2009b) shows root-mean-squared interannual variability in air–sea $CO_2$ flux of between $\pm 0.14$ and $\pm 0.29$ PgC yr$^{-1}$ for 1979–2004; however, the upper limit of variability represents a model run in which dust input was not allowed to vary interannually. Obata and Kitamura (2003) calculate interannual variability in the global air–sea $CO_2$ flux of $\pm 0.23$ PgC yr$^{-1}$ for 1961–1998, using a circulation–biogeochemistry model. Wetzel et al. (2005) calculate $1\sigma$ interannual variability of $\pm 0.25$ PgC yr$^{-1}$, based on a biogeochemical carbon cycle model coupled to a global ocean general circulation model, for 1948–2003. To the extent that these recent efforts overlap, the phasing between bottom-up estimates of the air–sea $CO_2$ flux variability appears to be reasonably consistent between studies, as well as with the bottom-up estimates that we use in this study (Lee et al., 1998; Le Quéré et al., 2003; Obata and Kitamura, 2003; Wetzel et al., 2005; Le Quéré et al., 2007; Park et al., 2010). The validity of bottom-up methods for calculating interannual variability in air–sea $CO_2$ flux is limited, however, by the spatial and temporal extent to which the relevant parameters (wind, $\Delta pCO_2$, etc.) can be continuously monitored, and considerable gaps exist in the timeseries of data used to calculate and model $CO_2$ fluxes in such key regions as, for example, the Southern Ocean (Doney et al., 2009a).

In this study, we use a new technique with a rearrangement of the traditional double deconvolution framework. Rather than parameterize disequilibrium flux and solve for the land and ocean fluxes (the double deconvolution), we instead pursue a thought experiment in which bottom-up estimates determine the interannual ocean flux variability, and calculate the disequilibrium

flux. Our goal is to investigate whether, assuming the bottom-up estimates of ocean $CO_2$ flux are correct, there are $\delta^{13}C$ budget parameters that are realistically adjustable so that atmospheric $\delta^{13}C$ observations can be reconciled with the low variability bottom-up ocean fluxes. Specifically, we attempt to solve for terrestrial disequilibrium flux, as well as one of the primary drivers of interannual variability in terrestrial disequilibrium flux: global flux-weighted terrestrial discrimination (hereafter referred to simply as discrimination). The focus of our study is on interannual variability, not flux magnitude.

As a caveat, we recognize that ocean flux variability may indeed be higher than suggested by ocean models and available empirical data. We use ocean flux estimates from empirical data and an ocean model, with $1\sigma$ standard deviations of $\pm 0.13$ PgC $yr^{-1}$ (Park et al., 2010) and $\pm 0.20$ PgC $yr^{-1}$ (Le Quéré et al., 2007), respectively. The results of Park et al. (2010) capture 70% of the interannual variability in ocean $CO_2$ fluxes, when compared with the data and modelling results of Doney et al. (2009b), and also show good agreement with ocean model results (Park et al., 2006). The model results of Le Quéré et al. (2007) represent the middle to upper range of interannual variability in air–sea $CO_2$ fluxes estimated from empirical and model studies (Lee et al., 1998; Le Quéré et al., 2003; Obata and Kitamura, 2003; Doney et al., 2009b). Although we have purposely employed a bottom-up air–sea $CO_2$ flux timeseries that represents relatively large interannual variability, it is certainly conceivable, given the limitations of current monitoring of relevant parameters, that air–sea flux variability is, in reality, larger than suggested by bottom-up studies (Doney et al., 2009a).

In light of such caveats to the viability of bottom-up ocean flux variability estimates, it is important to note the tight inverse correlation between the rate of change of atmospheric $CO_2$ and the $\delta^{13}C$ of atmospheric $CO_2$ (Fig. 1). This relationship suggests that year-to-year variability in atmospheric $\delta^{13}C$ is likely a predominantly terrestrial signal. Strong terrestrial uptake, and associated biological fractionation, lowers atmospheric $CO_2$ while simultaneously removing $^{12}C$ from the atmosphere. Therefore, the observation of a tight anti-correlation between atmospheric $CO_2$ and $\delta^{13}C$ suggests that variability in the airborne fraction is driven chiefly by the terrestrial biosphere. Measurements of $O_2/N_2$ also suggest that most of the recent interannual variability in the atmospheric $CO_2$ growth rate is due to variable terrestrial flux (Battle et al., 2000; Bender et al., 2005).

The primary objectives of this paper are as follows. We use a new technique, which we call the disequilibrium deconvolution, to investigate whether, in the limit of bottom-up ocean variability estimates, terrestrial carbon exchange mechanisms can realistically explain the observed interannual variability in atmospheric $^{13}CO_2$. The disequilibrium deconvolution has two steps. First, we calculate total global disequilibrium flux using bottom-up ocean fluxes and atmospheric observations as constraints. If ocean flux variability is as low as is suggested by bottom-up estimates, we find that global disequilibrium flux must have higher than expected interannual variability to satisfy atmospheric observations of $CO_2$ and $^{13}CO_2$. The second step is to 'deconvolve' the drivers of interannual variability in terrestrial $^{13}CO_2$ exchange; we explore as quantitatively as possible the potential contributions of various terrestrial processes. In doing so, we provide a new calculation of global disequilibrium flux and global terrestrial disequilibrium flux, as well as an estimate of global flux-weighted discrimination, and estimates of the extent to which $C_3/C_4$ vegetation shifts, disturbance, land use change, the $\delta^{13}C$ value of respired material and heterotrophic flux might contribute to the observed interannual variability in atmospheric $^{13}CO_2$.

We hope that this work will lay the foundation for future studies of terrestrial $^{13}CO_2$ exchange at higher spatial resolutions by providing a global context for the contributions of terrestrial carbon exchange to atmospheric $^{13}CO_2$ variability. As a global model, this method of exploring terrestrial $^{13}C$ flux variability is valuable because it obviates the need for horizontal and vertical atmospheric transport constraints, which can obscure results by adding uncertainty. Other recent studies have investigated the double deconvolution method by focusing on the sensitivity of $F_l$ and $F_o$ to changes in bottom-up calculations of the disequilibrium flux (e.g. Randerson et al., 2002; Scholze et al., 2008). This study is, by contrast, a top-down approach using the double deconvolution framework to constrain isotopic disequilibrium.

## 2. Methods

### 2.1. Measurement of $CO_2$ and $\delta^{13}C$

Top-down methods for measuring carbon cycle processes necessitate high-quality and spatially comprehensive atmospheric observations. The global Cooperative Air Sampling Network of the National Oceanic and Atmospheric Administration/Earth System Research Laboratory (NOAA/ESRL) is a collection of sampling sites, distributed globally, that monitor atmospheric $CO_2$ and $\delta^{13}C$. Regular measurements of carbon dioxide began in the 1950s with the establishment of monitoring stations in Antarctica, California and Hawaii (Keeling, 1960). Since NOAA/ESRL began a global network in 1967, the number of sites that monitor $CO_2$ has expanded to over 90. In 1990, regular measurements of $\delta^{13}C$ in atmospheric $CO_2$ also began. Figure 2 shows the locations of the NOAA/ESRL marine boundary layer (MBL) sites that contribute to the global means used in this study.

At NOAA/ESRL sites, two 2.2 l flasks are filled with air and sent to Boulder, Colorado, for analysis. Measurement of $CO_2$ concentrations, via non-dispersive infrared analysis, takes place at NOAA/Earth System Research Laboratories (ESRL), and measurement of $\delta^{13}C$, by dual inlet mass spectrometry, takes place at the University of Colorado Institute of Arctic and Alpine Research/Stable Isotope Lab (INSTAAR/SIL), both in Boulder, Colorado. $CO_2$ and $\delta^{13}C$ are measured to within $\pm 0.1$ ppm and

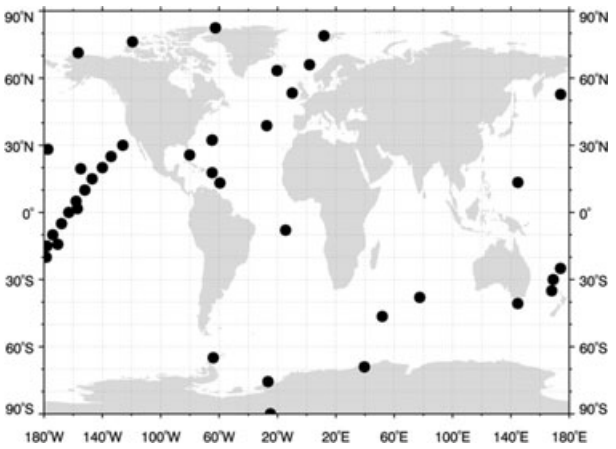


*Fig. 2.* Black dots show locations of surface monitoring sites in the NOAA/ESRL Cooperative Air Sampling Network that contribute marine boundary layer $CO_2$ and $^{13}CO_2$ measurements used to create global means in this study.

$\pm 0.012‰$, respectively ($1\sigma$, each). Duplicate flasks provide a means of quality control for data, and flasks with pair differences greater than three standard deviations are rejected. Conway et al. (1994), Trolier et al. (1996), Vaughn et al. (2004) and Vaughn et al. (2009) provide descriptions of sampling and analysis techniques.

One measure of data precision for $\delta^{13}C$ measurements is the repeated analysis of $CO_2$ extracted from whole air from a cylinder over time. These samples are treated as unknowns and are referred to as 'trap tanks'. Cylinders of air collected at Niwot Ridge, Colorado, are run as trap samples each time a set of flasks is analysed. From mid-2003 to 2009, the same trap tank (FRED-003) was run. During that time frame, four different reference gases were used. The plot in Fig. 3 shows that there was no significant drift and very low interannual variability in the data collected over this time period. A linear regression shows a statistically insignificant ($R^2 = 0.002$) trend of the trap values over this time indistinguishable from zero. This illustrates that calibration of $\delta^{13}C$ measurements on this machine is well maintained, and steady over long periods of time. Figure 3 also shows that the long-term scatter of the observations is consistent with a $1\sigma$ precision of 0.012‰. Furthermore, there is very low year-to-year variability in measurements of trap tank air. The $1\sigma$ standard deviation of the annual mean trap tank values is 0.0036‰ for 2003–2009. The greatest deviation of a mean annual value from the overall mean of the timeseries is 0.0062‰, and the greatest shift in the annual mean value from one year to the next occurs between 2004 and 2005: an increase of 0.0059‰. The significance of these results is that we can be sure that the atmospheric variability we measure and the disequilibrium flux variability we solve for are not artifacts of calibration variability.

The $CO_2$ and $\delta^{13}C$ observation data that we use in this study are smoothed and interpolated global averages from MBL NOAA/ESRL sites (Masarie and Tans, 1995). Smoothing in time is performed according to the methodology of Thoning et al. (1989), by producing a polynomial with a harmonic component for trends and annual variability, and filtering residuals for higher frequency variability.

### 2.2. *Single deconvolution*

The single deconvolution approach is a simple way to express the growth rate of atmospheric $CO_2$ in terms the relative contributions of the major surface exchanges (Siegenthaler and Oeschger, 1987). In eq. (1), the rate of change of atmospheric $CO_2$ ($dC_a/dt$) is controlled by the surface fluxes: fossil fuel combustion ($F_f$), net terrestrial biospheric exchange ($F_l$) and net oceanic exchange ($F_o$)

$$\frac{dCa}{dt} = F_f + F_l + F_o. \quad (1)$$

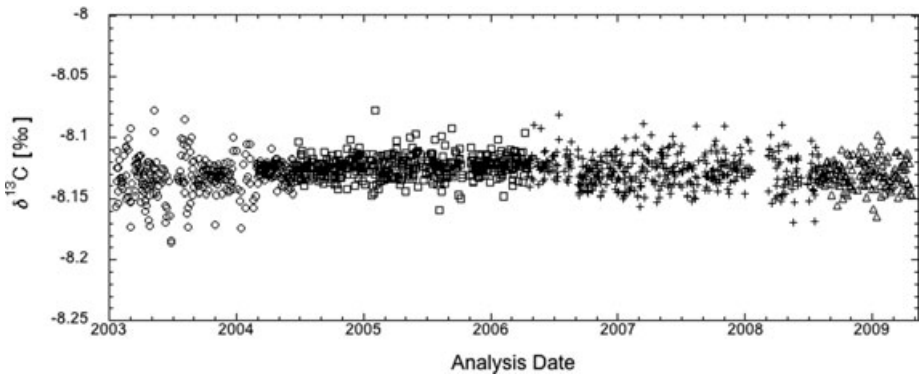


*Fig. 3.* Measured $\delta^{13}C$ values of air from the trap tank, FRED-003, run on the INSTAAR/SIL Optima dual-inlet mass spectrometer, Spock, over the course of four reference gas tanks: BRUN-003 (circles), DESI-005 (squares), NAGH-003 (plus signs), and BIGG-001 (triangles). Standard deviation for the data set is $\pm 0.012‰$, and a linear regression shows a statistically insignificant ($R^2 = 0.002$) trend of 9.6e−12‰ $yr^{-1}$, which, if real, would translate to an imperceptible drift over several decades. $1\sigma$ standard deviation of the annual mean trap tank values is 0.0036‰, suggesting interannual variability that is lower than run-to-run standard error.

In this approach, the rate of change of atmospheric $CO_2$ and the rate of fossil fuel combustion must be known, as well as one of the remaining reservoir exchange terms, either $F_l$ or $F_o$. For the purposes of this study, we specify bottom-up ocean fluxes as a 'known' constraint in the single deconvolution.

*2.2.1. Single deconvolution input parameters*. We use both model derived and empirically derived ocean fluxes to create timeseries of land and ocean fluxes, in order to represent the results of both of these approaches to estimating air–sea $CO_2$ fluxes. Ocean model results are from the Le Quéré et al. (2007) OPA General Circulation Model, which is coupled to the PISCES-T biogeochemistry model of Buitenhuis et al. (2006). Empirical ocean flux data are from Park et al. (2010), who extrapolate observed relationships between air–sea $CO_2$ flux climatology (Takahashi et al., 2009), sea surface temperatures, and windspeed anomalies. We propagate uncertainty in the ocean fluxes through our calculations and assess the implications for our findings. As another gauge of uncertainty, we examine the range in magnitude and variability between the Park et al. (2010) and Le Quéré et al. (2007) bottom-up fluxes. Also, note that because the single deconvolution budgeting technique solves for the land flux, $F_l$, as a residual of the other terms in eq. (1), it inherently includes carbon exchange fluxes from deforestation, reforestation and other land use changes.

### 2.3. $\delta^{13}C$ and the double deconvolution

The atmosphere is relatively well mixed, so the carbon dioxide mixing ratio can be considered an integration of the surface fluxes of this gas; it reflects the sum of the net fluxes from the land and ocean, and fossil fuel combustion, and its $^{13}C/^{12}C$ ratio reflects the sum of each gross surface flux multiplied by the kinetic and/or equilibrium fractionation occurring upon exchange. Because the product of $CO_2$ and $\delta^{13}C$ is conservative in the atmosphere (Tans, 1980), a mass balance equation can be written to express the rate of change of atmospheric $CO_2$ and $^{13}CO_2$ in terms of net surface $CO_2$ fluxes and their associated fractionation factors (Ciais et al., 1995).

This isotopic mass balance equation mirrors eq. (1), but rather than expressing the rate of change of $CO_2$, it expresses the atmospheric $\delta^{13}C$ growth rate (Tans et al., 1993)

$$C_a \frac{d\delta_a}{dt} = (\delta_f - \delta_a)F_f + \varepsilon_{ab}F_l + \varepsilon_{ao}F_o + (\delta_{ba} - \delta_{ab})F_{ba} + (\delta_{oa} - \delta_{ao})F_{oa}, \quad (2)$$

where $\delta_a$ is the $\delta^{13}C$ value of atmospheric $CO_2$ and $\delta_f$ is the $\delta^{13}C$ signature of fossil fuel emissions. $\varepsilon_{ab}$ and $\varepsilon_{ao}$ are the kinetic fractionation factors for photosynthesis and ocean ingassing, respectively. $F_{ba}$ and $F_{oa}$ are the gross one-way $CO_2$ fluxes from the reservoir indicated by the first subscript to that indicated by the second (a is atmosphere, b is terrestrial biosphere and o is ocean). $\delta_{ba}$, $\delta_{ab}$, $\delta_{oa}$ and $\delta_{ao}$ are the isotopic signatures of the one-way carbon exchange between the reservoir indicated by the first subscript and that indicated by the second. An approximation of this relationship (neglecting a small error arising from the conversion from $R$, the molar ratio of $^{13}C/^{12}C$, to $\delta$) is

$$\delta_{ab} = \varepsilon_{ab} + \delta_a. \quad (3)$$

A complication of using $\delta^{13}C$ to close the $CO_2$ budget is the disequilibrium flux (eqs. 4a and b). Note that here we use the term 'disequilibrium flux' (in units of PgC‰ $yr^{-1}$) for $D_l$, $D_o$, or their sum, and the term 'isodisequilibrium forcing coefficient' (in units of ‰) to refer to ($\delta_{xa}$–$\delta_{ax}$). Photosynthesis and respiration are not contemporaneous, and because the $\delta^{13}C$ of atmospheric $CO_2$ is being continuously depleted through the burning of $^{12}C$-rich fossil fuels (the $^{13}C$ Suess Effect: Keeling, 1979), an isotopic disequilibrium arises from $CO_2$ moving into and out of the ocean and land reservoirs. This term is not negligible, thus land and ocean disequilibrium fluxes ($D_l$ and $D_o$, respectively) must be accounted for in any attempt to budget atmospheric $CO_2$ using isotopes. In eq. (2), the land and ocean disequilibrium fluxes are represented by the penultimate and ultimate terms, respectively. It is important to note that for the purposes of calculating disequilibrium flux, $F_{ba}$ is taken only as heterotrophic respiration and fire fluxes, that is, the oxidation to $CO_2$ of biospheric carbon with a significant age. It is likely that there is no disequilibrium associated with autotrophic respiration of $CO_2$ because of its very short residence time (e.g. Bowling et al., 2002).

$$D_l = (\delta_{ba} - \delta_{ab})F_{ba}, \quad (4a)$$

$$D_o = (\delta_{oa} - \delta_{ao})F_{oa}. \quad (4b)$$

As in eq. (1), $\delta_{xa}$ and $\delta_{ax}$ are the isotopic signatures of the one-way carbon exchanges between the atmosphere and surface reservoir (eq. 3). Together, these terms represent the isodisequilibrium forcing coefficient, ($\delta_{xa}$–$\delta_{ax}$), or the factor by which, in the case of $D_l$, discrimination upon biospheric $CO_2$ uptake and biospheric residence time of $CO_2$ control the isotopic magnitude of the disequilibrium flux. The respiration flux, $F_{ba}$, controls the mass of carbon in isotopic disequilibrium because it is the amount of old carbon (assimilated from an isotopically 'heavier' atmosphere) exported to the modern atmosphere. The respiration flux and the isodisequilibrium forcing coefficient each modulate the impact that the other can have on total terrestrial disequilibrium flux. The equivalent processes hold true for $D_o$.

In the double deconvolution technique, eqs. (1) and (2) are combined to solve for the net land and ocean $CO_2$ fluxes ($F_l$ and $F_o$) simultaneously (Keeling et al., 1989; Ciais et al., 1995; Joos and Bruno, 1998).

*2.3.1. Double deconvolution input parameters*. Atmospheric $CO_2$ and $\delta^{13}C$ observations ($C_a$ and $\delta_a$) are from the NOAA/ESRL Global Monitoring Division sites shown in Fig. 2. Fossil fuel and cement production data ($F_f$) are compiled with data from Carbon Dioxide Information Analysis Center (CDIAC) (Boden et al., 2009) and BP (BP Statistical Review of World Energy June, 2009). Yearly $\delta_f$ estimates are derived from

CDIAC fuel type use data, $\varepsilon_{ao}$ is fixed at $-2‰$ (Zhang et al., 1995) and $\varepsilon_{ab}$ is generated by the SiB2 biosphere model (Suits et al., 2005). As in the single deconvolution, terrestrial carbon exchange from deforestation, reforestation and other land use changes are included in $F_l$.

Seasonally variable, but interannually repeating terrestrial discrimination is modelled using the SiB2 framework, in combination with empirically derived relationships between stomatal conductance and climatic parameters (Suits et al., 2005). This formulation accounts for the presence of both $C_3$ and $C_4$ photosynthetic pathways according to the satellite derived land cover maps of Still et al. (2003). To derive a global average discrimination, we weight the discrimination by SiB net assimilation in each month and 1° grid cell.

Estimating the disequilibrium flux requires knowledge of the time history of atmospheric $\delta^{13}C$ depletion due to the Suess Effect, the residence time of carbon in the reservoir of interest, and a time history of the amount and $\delta^{13}C$ signature of carbon respired from that reservoir. Spatially and temporally resolved estimates of disequilibrium flux can therefore be made using bottom-up techniques to estimate these parameters.

Terrestrial disequilibrium flux is estimated using impulse-response functions from the Carnegie Ames Stanford Approach (CASA) model (Thompson and Randerson, 1999) and the paleo-atmospheric history of $CO_2$ (Etheridge et al., 1996) and $\delta^{13}C$ (Francey et al., 1999), in combination with modern NOAA/ESRL and CU/INSTAAR observations. The CASA impulse-response functions can be transformed to an age distribution of heterotrophic respiration in each $1° \times 1°$ terrestrial grid cell. This age distribution can be convolved with the atmospheric history of $CO_2$ and $\delta^{13}C$ to give the isodisequilibrium forcing coefficient ($\delta_{ba}-\delta_{ab}$). In this calculation, photosynthetic isotopic fractionation is assumed to be constant. The CASA impulse-response functions also give total heterotrophic respiration, $F_{ba}$. Time trends in $D_l$ are calculated simply by repeating the calculation for an additional year and adding 1 year to the time trends of atmospheric $\delta^{13}C$ and $CO_2$.

The analogous ocean disequilibrium flux, $D_o$, is estimated using observations of the surface ocean $pCO_2$ (Takahashi et al., 2009) in conjunction with the $\delta^{13}C$ value of surface ocean dissolved inorganic carbon (DIC) (Gruber et al., 1999). The gross ocean–atmosphere flux, $F_{oa}$, is calculated using surface ocean $pCO_2$ and the quadratic windspeed-based gas exchange formulation of Wanninkhof (1992), using windspeed, temperature, salinity and sea-ice fields provided by Takahashi. The isodisequilibrium forcing coefficient, ($\delta_{oa}-\delta_{ao}$), is calculated using the surface ocean $\delta^{13}C$ of DIC and a temperature-dependent equilibrium fractionation formulation (Zhang et al., 1995), compared with the atmospheric $\delta^{13}C$ as a function of latitude and season. Both the surface ocean $pCO_2$ and $\delta^{13}C$ data products are seasonal climatologies. To estimate timeseries for isotopic disequilibrium flux, we need to extrapolate these climatologies in time. For $pCO_2$, we use the original recommendation of Takahashi et al. (1997), that $\Delta pCO_2$ is constant in the mid-latitude gyres (roughly south of 40°N), while $pCO_2$ is constant towards the poles. For $\delta^{13}C$ of DIC we use trends in 10° latitude zones from Gruber et al. (1999). Neither the $pCO_2$, nor $\delta^{13}C$ climatologies and trends account for changes in $pCO_2$, $\delta^{13}C$ of DIC, SST or windspeed associated with ENSO. However, trends calculated agree well with the Hawaiian Ocean Timeseries (HOT) and Bermuda Atlantic Timeseries Study (BATS) of $\delta^{13}C$ and $CO_2$. For the calculations in this paper, both $D_l$ and $D_o$ are summed globally, but retain their temporal trends.

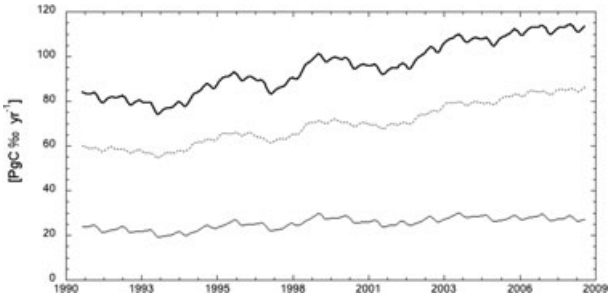


*Fig. 4.* Global 12-month mean total (bold line), ocean (dotted line) and land (fine line) disequilibrium flux, based on the CASA model, and surface ocean $pCO_2$ and $\delta^{13}C$, as described in Section 2.3.1. The disequilibrium fluxes shown have been scaled up by 30%, as described in Section 2.3.1.

Figure 4 shows total, ocean and land disequilibrium flux, as derived using the methods described in this section. These bottom-up estimates are scaled by a factor of 1.3 for use in the double deconvolution by multiplying each timeseries by a factor of 1.3. The choice of 1.3 does not significantly impact our conclusions, because we focus only on the issue of interannual variability. The scaling factor was chosen because, in a double deconvolution, it produces land and ocean $CO_2$ flux magnitudes that are closer to the results of recent carbon cycle budgeting studies. A useful metric for comparison is the Global Carbon Project's (GCP) 'Carbon Budget and Trends 2008', because the ocean model that is used to calculate the GCP budget is the same as that cited in this study (Le Quéré et al., 2007, 2009). The GCP estimates an average net ocean $CO_2$ sink of 2.3 PgC $yr^{-1}$ for 2000–2008 (Le Quéré et al., 2009). When the unscaled disequilibrium flux is used in the double deconvolution, with all other inputs as described earlier, the resulting average ocean sink is 0.36 PgC $yr^{-1}$, whereas the double deconvolution using disequilibrium flux scaled by 1.3 results in an average ocean sink of 2.0 PgC $yr^{-1}$ for 2000–2008. The GCP budget estimates the average net terrestrial $CO_2$ sink (minus losses due to land use change) to be roughly 1.5 PgC $yr^{-1}$ (Le Quéré et al., 2009), on average, for 2000–2008. Double deconvolution using the unscaled disequilibrium flux yields an average net land sink of 3.3 PgC $yr^{-1}$ for 2000–2008. When the disequilibrium flux is scaled by a factor of 1.3, the average net land sink produced by the double deconvolution is 1.7 PgC $yr^{-1}$ for 2000–2008.

This example makes evident that increasing our bottom-up disequilibrium flux by 30% before using it in the double deconvolution produces land and ocean $CO_2$ fluxes that are much closer in magnitude to the GCP estimate. Furthermore, as will be shown in the results section of this paper, the scaled disequilibrium flux is of the same magnitude as the total global disequilibrium flux that we calculate using the disequilibrium deconvolution.

### 2.4. Disequilibrium deconvolution

Our limited ability to make confident estimates of land and ocean disequilibrium flux is a major drawback to the double deconvolution method. In their double deconvolution studies, Ciais et al. (1995) and Keeling et al. (1989) both treated the disequilibrium flux as a constant trend responding only to the Suess Effect. Other double deconvolution-style techniques have used the same assumption (Quay et al., 1992; Enting et al., 1993, 1995; Tans et al., 1993; Francey et al., 1995; Keeling et al., 1995; Joos and Bruno, 1998). It has long been known that this assumption was flawed, however, because interannual variability in photosynthetic discrimination (a primary factor affecting $\varepsilon_{ab}$) exists (Farquhar et al., 1982; Collatz et al., 1991; Lloyd and Farquhar, 1994). In the double deconvolution, the 'indirect' sensitivity of $F_l$ and $F_o$ to $\varepsilon_{ab}$, that is, sensitivity via the presence of $\varepsilon_{ab}$ in $D_l$ (eqs. 3 and 4a), is large. This is because $\delta_{ab}$, which varies with $\varepsilon_{ab}$ according to eq. (3), is multiplied by $F_{ba}$, which is of order 50 PgC yr$^{-1}$.

Randerson et al. (2002) amended the traditional double deconvolution inversion to allow $C_3$ plant discrimination to vary linearly with gross primary productivity, within a range of 0.4‰. The result was less variable ocean fluxes than previous double deconvolution solutions, indicating that the use of time-varying rather than constant $C_3$ plant discrimination in calculating bottom-up disequilibrium flux has the potential to at least partially reconcile atmospheric observations with bottom-up estimates of ocean surface flux variability.

In the disequilibrium deconvolution, we turn the traditional double deconvolution around. Rather than specifying disequilibrium flux and solving for $F_l$ and $F_o$, we specify $F_o$ according to two bottom-up estimates, and solve for disequilibrium flux. The first step toward solution of the disequilibrium deconvolution is to use bottom-up ocean flux in eq. (1) to solve for $F_l$. $F_l$ and $F_o$ are then be used as inputs into a simple rearrangement of eq. (2), which yields an expression for total disequilibrium flux as a residual of the other budget terms, where $D_{tot} = D_l + D_o$

$$D_{tot} = C_a\left(\frac{d\delta_a}{dt}\right) - F_f(\delta_f - \delta_a) - \varepsilon_{ab}F_l - \varepsilon_{ao}F_o. \quad (5)$$

*2.4.1. Disequilibrium deconvolution input parameters.* The input parameters for the disequilibrium deconvolution include those described for the double deconvolution (Section 2.3.1) for $C_a$, $\delta_a$, $F_f$, $\delta_f$, $\varepsilon_{ab}$ and $\varepsilon_{ao}$. $F_o$ is from the two bottom-up ocean flux estimates that were used in the single deconvolution (Section 2.2.1): ocean model results are from Le Quéré et al. (2007), and empirical ocean flux data are from Park et al. (2010). As described earlier, $F_l$ is calculated using these parameters in eq. (1).

## 3. Results and discussion

### 3.1. Single versus double deconvolution results

In this study, we focus specifically on interannual variability in $CO_2$ and $^{13}C$ fluxes. Of less concern is the absolute magnitude of the ocean and land sinks, as we have tuned the double deconvolution results to align with the magnitude of the ocean model results by multiplying bottom-up disequilibrium flux calculations by a factor of 1.3.

It is reasonable to increase our bottom-up disequilibrium flux calculation by 30%, given that the differences in magnitude of different model solutions for disequilibrium flux are of the same order. Thompson and Randerson (1999) convolve impulse-response functions of two terrestrial carbon cycle models with historical records of atmospheric $\delta^{13}C$ to calculate timeseries of terrestrial disequilibrium. They find that when different carbon-input references are used, calculated disequilibrium flux varies by up to 30% (Fig. 12 in Thompson and Randerson, 1999). The difference is even greater when a different model is used to create the impulse-response function. Given that there remains a lack of consensus regarding which carbon-input reference is preferable (gross primary productivity vs. net primary productivity), a 30% modulation in our bottom-up disequilibrium flux (which is calculated using the same technique as Thompson and Randerson) is reasonable. It is clearly evident that the scaling factor eases comparison between different approaches, and that a scaling factor of 1.3 is within the bounds of uncertainty in bottom-up calculations of disequilibrium flux. Moreover, as we demonstrate in Section 3.2, this scaling factor does not affect our conclusions regarding interannual variability in $^{13}CO_2$.

Figure 5 shows the results of the single (Fig. 5a) and double deconvolutions (Fig. 5b). Both the single and double deconvolution land–air $CO_2$ fluxes show substantial interannual variability, with slightly greater year-to-year variability in the double deconvolution $F_l$. The standard deviations of the annual mean land fluxes for the double deconvolution, Park et al. (2010) single deconvolution, and Le Quéré et al. (2007) single deconvolution are 1.39, 1.14, and 1.12 PgC yr$^{-1}$, respectively (all $1\sigma$). The phasing of the double deconvolution land flux corresponds closely to that of the two single deconvolution land fluxes. Furthermore, the net land–air $CO_2$ fluxes from all three simulations show similar features to other top-down $CO_2$ inversions (e.g. Bousquet et al., 2000; Rodenbeck et al., 2003; Baker et al., 2006). Notable examples of terrestrial sink anomalies that are evident in other atmospheric inversions include an increased sink in 1992

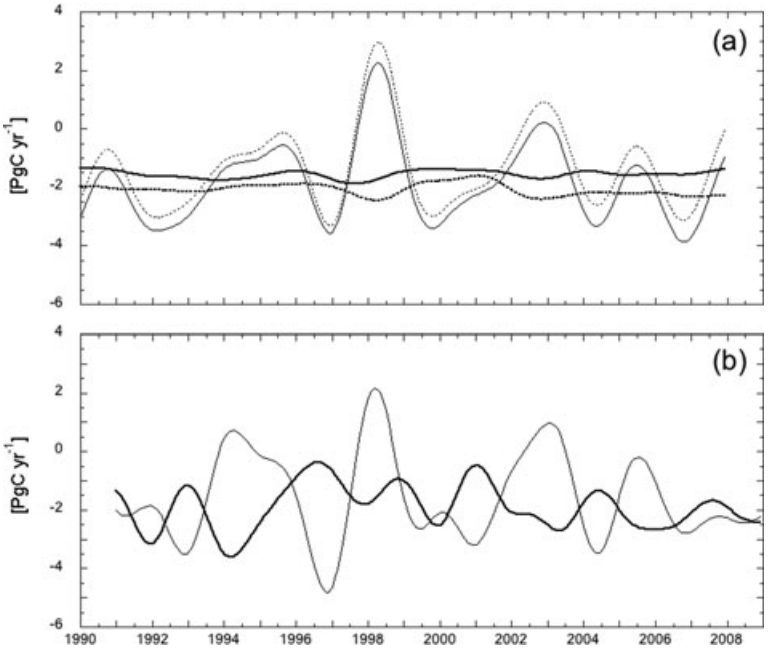


*Fig. 5.* (a) Net land flux (fine dotted line) derived using ocean fluxes (bold dotted line) of Le Quéré et al. (2007), and net land flux (fine solid line) derived using ocean fluxes (bold solid line) of Park et al. (2010). (b) Net ocean (bold line) and land (fine line) $CO_2$ fluxes derived from the double deconvolution (see text for details). Negative values indicate a sink for atmospheric $CO_2$.

following the eruption of Mt. Pinatubo, and a greatly increased source in 1997–1998 during the strong El Niño. Terrestrial flux variability maps onto processes that would be expected to cause changes in fluxes; for example, bottom-up models predict the terrestrial emissions calculated during 1997–1998, as this was a strong El Niño year and much of the tropical biosphere underwent drying and biomass burning (Page et al., 2002; van der Werf et al., 2004). It is also notable that there is no discernible trend in either the double or single deconvolution results from 1990 to 2008.

The most striking feature of Fig. 5 is that interannual bottom-up ocean flux variability (Fig. 5a) is much lower than interannual double deconvolution ocean flux variability (Fig. 5b). The standard deviation of the double deconvolution ocean flux timeseries is 0.82 PgC yr$^{-1}$, whereas the standard deviation of the Park et al. (2010) ocean flux timeseries is 0.13 PgC yr$^{-1}$ and that of the Le Quéré et al. (2007) ocean flux timeseries is 0.20 PgC yr$^{-1}$ (all $1\sigma$). This finding, that ocean flux variability calculated using the traditional double deconvolution approach is significantly larger than that estimated with bottom-up methods, is not new. Joos and Bruno (1998), for example, found that ocean carbon uptake calculated using a double deconvolution approach displayed high variability between 1950 and 2000, whereas the results of an ocean–atmosphere model were significantly smoother.

Another concern in the results of the atmospheric double deconvolution approach is that the land and ocean fluxes display a notable anti-correlation. In mass balance calculations solving for two unknowns, anti-correlations can signify a problem because, as is the case in eqs. (5) and (1), errors in the solution of one term ($F_l$) are translated to the solution of the second term ($F_o$), in a seesaw fashion. As is more completely discussed in Section 3.6, however, the phasing of the single deconvolution ocean flux is similar to that of the double deconvolution ocean flux, and both show a tendency towards anti-correlation with the net terrestrial $CO_2$ flux. Although the anticorrelation is less notable in the single deconvolution than in the double deconvolution, the similar phasing of these two independent measures suggests that some of the anti-correlation between the double deconvolution ocean and land fluxes may be real.

### 3.2. *Deconvolving the disequilibrium flux results*

The aim of our study is not only to produce a new 'top-down' timeseries of total global disequilibrium flux, but also to investigate whether the resulting variability in this term is reasonable, given what we know about the processes controlling surface $^{13}C$ cycling. In particular, we are interested in investigating the primary contributors to the terrestrial disequilibrium flux. To that end, our first step in analysing the disequilibrium flux result from our disequilibrium deconvolution, or 'deconvolving' the drivers of disequilibrium flux variability, is to isolate the ocean and terrestrial biosphere components. For ease of discussion, we hereafter refer to the disequilibrium flux calculated using the disequilibrium deconvolution as 'top-down' disequilibrium flux, although the reader should be aware that this term is imprecise, as the disequilibrium flux is constrained, in part, by bottom-up ocean fluxes.

An interannually varying, bottom-up estimate of scaled ocean disequilibrium flux is removed from the total disequilibrium flux to isolate the land disequilibrium flux. To test the sensitivity of terrestrial disequilibrium flux to different methods of scaling the ocean disequilibrium flux, before its subtraction from the

total disequilibrium flux, we scale to a constant global total of 100 PgC‰ $yr^{-1}$, scale to a global trend of 90–110 PgC‰ $yr^{-1}$ over the decade of interest, and leave the original bottom-up ocean disequilibrium flux as is, unscaled. These different methods of scaling (or lack of scaling) do not result in a significant difference in the interannual variability of terrestrial disequilibrium flux from the 1.3 scaling method. As with the naming of our 'top-down' disequilibrium flux, we hereafter refer to the resulting terrestrial disequilibrium flux calculation as 'top-down', even though it is the solution of calculations using bottom-up ocean fluxes as well as bottom-up ocean disequilibrium fluxes.

The terrestrial disequilibrium flux timeseries, now isolated from the total disequilibrium flux, is a potentially powerful diagnostic tool for two reasons. First, it represents an integration of interannual changes in biospheric carbon exchange dynamics that, if unraveled, could yield a new view into the controls on terrestrial $^{13}CO_2$ as well as $CO_2$ cycling over annual to interannual timescales. The second diagnostic quality of our calculated disequilibrium flux is that it is a quasi-independent gauge of the reliability of bottom-up ocean flux variability. That is, if interannual variability in our calculated terrestrial disequilibrium flux is far outside of the bounds of what could be expected from examination of biospheric processes, then this result would indicate that either some other component of the carbon cycle must account for the observed discrepancy between single and double deconvolution results, or that ocean variability is greater than previously thought.

We investigate several potential drivers of year-to-year variability in terrestrial disequilibrium flux. We test and discuss the sensitivity of terrestrial disequilibrium flux to the potential host of processes that could control $D_l$ variability: the $\delta^{13}C$ value of newly formed plant matter ($\delta_{ab}$), heterotrophic respiration and fire ($F_{ba}$), the residence time of carbon in the terrestrial biosphere and the $\delta^{13}C$ value of respired carbon ($\delta_{ba}$).

We then shift our focus to a more thorough examination of how and why $\delta_{ab}$ might vary from year to year, and the extent to which $\delta_{ab}$ variability could contribute to our calculated terrestrial disequilibrium flux variability. Interannual variability in global flux weighted discrimination, as a result of $C_3$ stomatal conductance and the relative activity of $C_3$ and $C_4$ vegetation, has, in the past, been shown to be a primary driver of terrestrial disequilibrium flux variability (Randerson et al., 2002; Scholze et al., 2008). To investigate the likelihood that discrimination can explain our calculated terrestrial disequilibrium flux variability, we solve for discrimination using a few assumptions. First, the annual heterotrophic respiration flux is held constant at 50 Pg $yr^{-1}$, and allowed to vary seasonally by scaling monthly totals to assimilation produced by SiB2. Second, the isotopic signature of heterotrophic respiration, $\delta_{ba}$, is assumed to have a constant value of −23‰, with no interannual variability.

### 3.3. Disequilibrium flux results

It is evident from our ocean/atmosphere constrained calculation of disequilibrium flux that when prescribed bottom-up ocean $CO_2$ fluxes have relatively low interannual variability (as do those of Le Quéré et al., 2007 and Park et al., 2010), the resulting global disequilibrium flux, $D_{tot}$, has very high interannual variability (Fig. 6). Global mean disequilibrium flux from 1991 to 2007 is 100.2 PgC‰ $yr^{-1}$ when calculated with the Le Quéré et al. (2007) ocean fluxes, and is 92.3 PgC‰ $yr^{-1}$ when calculated with the Park et al. (2010) ocean fluxes. To investigate interannual variability, we first remove the trend in the disequilibrium flux. After detrending, the $1\sigma$ residual standard deviation is 13.0 PgC‰ $yr^{-1}$ when calculated using the Le Quéré et al. (2007) ocean fluxes, and 12.6 PgC‰ $yr^{-1}$ when calculated using the Park et al. (2010) ocean fluxes. In contrast, the $1\sigma$ residual standard deviation of the bottom-up disequilibrium flux, after detrending, is 3.6 PgC‰ $yr^{-1}$.

We find an increasing trend through time in total disequilibrium flux of 2.0 PgC‰ $yr^{-1}$ per year when calculated using the Park et al. (2010) ocean fluxes, and 2.4 PgC‰ $yr^{-1}$ per year when calculated using the Le Quéré et al. (2007) ocean fluxes, for 1991–2007. The increase in the magnitude of global

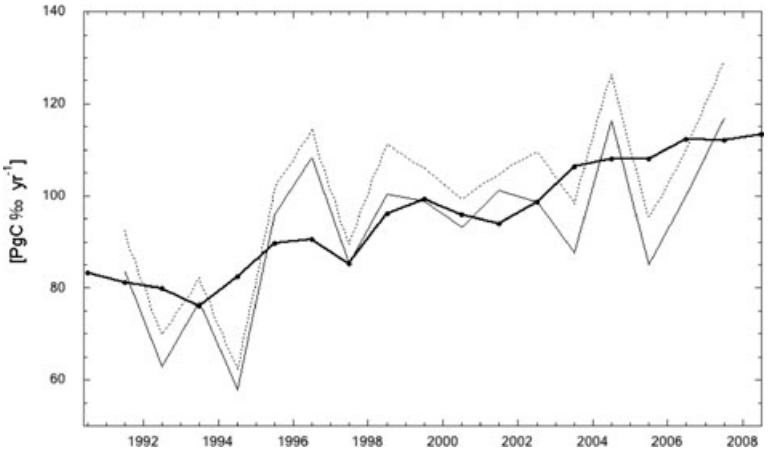


*Fig. 6.* Annual mean total global disequilibrium flux, calculated with eqs. (1) and (5), and the ocean fluxes of Park et al. (2010) (fine black line) and Le Quéré et al. (2007) (fine dotted line). Solid black line with markers is bottom-up annual mean total global disequilibrium flux, scaled by 30%, as in Fig. 4.

disequilibrium flux, which has been noted by others, is the result of increased fossil fuel burning, which widens the $\delta^{13}C$ difference between $CO_2$ assimilated and released from the oceans and terrestrial biosphere each year (Joos and Bruno, 1998; Scholze et al., 2008). The trend that we calculate from a top-down perspective is similar to that estimated from a bottom-up perspective; we calculate an increasing trend of 2.1 PgC‰ $yr^{-1}$ per year from 1990 to 2008 in our bottom-up disequilibrium flux. That the bottom-up and top-down trends agree suggests that the fossil fuel Suess Effect, which is what drives the bottom-up trend, is also the reason for the trend in the top-down disequilibrium flux.

### 3.4. *Explanations of top-down disequilibrium flux variability*

We find that placing a limit on interannual ocean flux variability (by using bottom-up estimates) results in an increase in disequilibrium flux variability. We define a new term, 'residual isotopic variability', to clarify discussion of the impact of the disequilibrium deconvolution budgeting technique on inferred isotopic variability of different parts of the carbon cycle. Current process-based estimates of the impact of surface $^{13}CO_2$ exchanges on $\delta_a$ cannot reproduce the magnitude of observed interannual variability in the rate of change of $\delta_a$, hence residual isotopic variability. Residual isotopic variability can be thought of as the timeseries of $\delta_a$ residuals, or anomalies, that would be left unaccounted for if all of the current bottom-up estimates of fossil fuel, land, ocean and disequilibrium fluxes were combined and subtracted from the observed atmospheric $\delta^{13}C$ growth rate.

In the disequilibrium deconvolution, a closed budgeting technique, residual isotopic variability is expressed in the disequilibrium flux (Fig. 6), because it is the only term in eq. (5) that can reasonably absorb such high year-to-year changes. All other would be sources of variability are unlikely to contribute substantially to the residual isotopic variability for one or more of the following reasons.

First, several of the input parameters are well enough constrained that fluctuations large enough to contribute (in any significant way) to the residual isotopic variability would be outside of their bounds of error. Fossil fuel fluxes and their $\delta^{13}C$ values are known to within 10%. Atmospheric $CO_2$ mixing ratios are known to within 0.1 ppm, and, as discussed earlier, interannual variability in atmospheric $\delta^{13}C$ is unlikely to be greater than 0.012‰ different from that observed. The solution of eq. (2) for $d\delta_a/dt$ shows that interannual variability of 0.63‰ $yr^{-1}$ would be required if the disequilibrium flux were specified as in Fig. 4. Given $\delta_a$ measurement certainty of ±0.012‰, and the observation that, from 1991 to 2007 the standard deviation of $d\delta_a/dt$ was only 0.027‰ $yr^{-1}$, we conclude that measurement error is very unlikely to contribute significantly to the residual isotopic variability that we calculate. Similarly, the fractionation of $^{13}CO_2$ upon uptake by the oceans is well measured in laboratory settings (Zhang et al., 1995), and, as Tans et al. (1993) discuss in depth, it is doubtful that $\varepsilon_{ao}$ in the real world deviates very much from this laboratory established value.

Second, net ocean and land $CO_2$ fluxes are constrained by design of our method; the goal of our study is to investigate other possible sources of variability, in the limit of bottom-up ocean flux estimates. It is conceivable, however, that there is greater year-to-year variability in ocean fluxes than is predicted by the bottom-up ocean estimates that we use.

Uncertainty in bottom-up estimates of ocean $CO_2$ fluxes stems largely from uncertainty in the parameterization of the relationship between gas transfer velocity and windspeed, or scaling factor (Olsen et al., 2005; Krakauer et al., 2006; Naegler et al., 2006; Sweeney et al., 2007). Uncertainty in the air–sea $CO_2$ flux from the Le Quéré et al. (2007) model is ±0.4 PgC $yr^{-1}$ for the period from 1990 to 2000 (Canadell et al., 2007). In comparison, the Ocean Model Intercomparison Project (OCMIP) found an uncertainty of ±0.35 PgC $yr^{-1}$ between four model calculations of global ocean $CO_2$ uptake for the 1980s (Orr et al., 2001). Because the OCMIP models shared input parameters, additional uncertainties from gas exchange and surface alkalinity were not expressed in the inter-model uncertainty, but could add ±0.1 PgC $yr^{-1}$ uncertainty each (Le Quéré et al., 2003). Uncertainty in the Le Quéré et al. (2007) model results is therefore within the range of the OCMIP model uncertainties.

The uncertainty of empirical flux estimates is difficult to evaluate (Park et al., 2006). In addition to the factors mentioned earlier, uncertainty in the sea–air $pCO_2$ difference ($\Delta pCO_2$) can affect the reliability of observationally based bottom-up ocean $CO_2$ flux estimates (Takahashi et al., 2009). Taking into account the influences of both $\Delta pCO_2$ and the choice of a scaling factor, as well as the uncertainties inherent in sampling and interpolation, wind speeds, and the calculated mean rate of change of $pCO_2$ (for normalization to the year 2000), Takahashi et al. (2009) calculated the global ocean $CO_2$ flux and uncertainty to be $-2 \pm 1.0$ PgC $yr^{-1}$ for 2000 by using $pCO_2$ flux climatology. Sweeney et al. (2007), also using $pCO_2$ climatology, calculate a flux and uncertainty of $-1.8 \pm 0.5$ PgC $yr^{-1}$ for 1995. Naegler et al. (2006), using similar methods, calculate an ocean flux of $-1.57 \pm 0.30$ PgC $yr^{-1}$ for 1995.

The uncertainty of the Le Quéré et al. (2007) ocean fluxes, ±0.4 PgC $yr^{-1}$, is comparable to other modelling studies and $pCO_2$ climatology studies. When we propagate ocean flux uncertainty of ±0.4 PgC $yr^{-1}$ through our calculations, we find that this results in an uncertainty of ±6.0 PgC‰ $yr^{-1}$ in total global disequilibrium flux (when calculated using both bottom-up ocean fluxes), on average from 1991 to 2007. The absolute differences between average sink strengths are not, however, a matter of direct concern for the purposes of our investigation. We are interested in calculating interannual variability in disequilibrium flux and unravelling its controls, not constraining its absolute magnitude. We find that changing the ocean flux by ±0.4 PgC $yr^{-1}$ has an imperceptible influence on the

interannual variability in the disequilibrium flux. Because changing the magnitude of the ocean flux does not affect interannual variability in disequilibrium flux, we take the difference in interannual variability between the two bottom-up ocean fluxes (Le Quéré et al., 2007; Park et al., 2010) as more representative of the effect that uncertainty in ocean fluxes can have on disequilibrium flux variability. As discussed in Section 1, we find that the Park et al. (2010) and Le Quéré et al. (2007) ocean fluxes are, together, a good representation of the possible range in interannual variability found by other studies, and that the Le Quéré et al. (2007) estimate represents the upper range of ocean flux variability estimated by bottom-up methods.

Finally, the remaining input parameters lack the necessary leverage, as coefficients in our equations, to contribute in any substantial way to residual isotopic variability. As discussed in Section 2.4, the 'indirect' sensitivity of disequilibrium flux to changes in $\varepsilon_{ab}$ is large. The value of the disequilibrium deconvolution is that this 'indirect' sensitivity is not expressed in eq. (5); $\varepsilon_{ab}$ fluctuations are solved for, not parameterized, in our approach. In eq. (5), $\varepsilon_{ao}$ and $\varepsilon_{ab}$ hold little clout as factors. Therefore, the 'direct' sensitivity of our results to changes in $\varepsilon_{ab}$ and $\varepsilon_{ao}$, via multiplication of the net land and ocean fluxes, is quite small. Although the gross land and ocean exchange fluxes are of order 100 PgC yr$^{-1}$ (Denman et al., 2007), the net fluxes by which $\varepsilon_{ao}$ and $\varepsilon_{ab}$ are multiplied are on the order of only a few PgC yr$^{-1}$ in eq. (5).

### 3.5. *Physical explanations of disequilibrium flux variability*

The interannual variability in disequilibrium flux that we calculate using the disequilibrium deconvolution (Fig. 6) is much larger than that expected based only on the Suess Effect. In Section 3.4, we investigated justifications for the expression of residual isotopic variability in disequilibrium flux by examining the extent to which variability or uncertainty in other terms in eq. (5) could contribute to residual isotopic variability. We find that disequilibrium flux is the only term in the disequilibrium deconvolution that can realistically contribute to such high residual isotopic variability. We now ask whether the implied interannual variability in disequilibrium flux is plausible, given our understanding of the processes governing terrestrial $^{13}$C cycling. If these results are not believable, then we must question our basic assumption that the bottom-up ocean fluxes are indeed as invariant as presumed. Bottom-up model results can only truly be reconciled with atmospheric observations if reasonable physical explanations can be found for the difference in interannual variability between 'top-down' disequilibrium flux, calculated via the disequilibrium deconvolution, and bottom-up disequilibrium flux (Fig. 6).

Although the oceans contribute a greater proportion of total global disequilibrium, we look to land disequilibrium flux as the primary contributor to interannual variability in total disequilibrium flux for two reasons. First, the generally shorter residence times of carbon in the terrestrial biosphere, and the greater volatility of this reservoir in response to synoptic and smaller scale perturbations, make it a more likely source of interannual variability in $D_{tot}$. We discuss the relevant mechanisms and the range of their potential contributions to observed variability later. Second, in keeping with the basic theme of this investigation, we choose to proceed by assuming that bottom-up estimates of the oceanic contribution to atmospheric $CO_2$ and $\delta^{13}$C variability are sound. However, although most signs point to terrestrial disequilibrium flux as the primary driver of interannual variability in total disequilibrium flux, we cannot rule out the possibility that interannual windspeed variability over the Southern Ocean, for example, in conjunction with other factors, contributes to more variable ocean disequilibrium than is allowed for by our bottom-up calculation. For the purposes of this thought experiment, we operate under the assumption that the scaled bottom-up estimates of ocean disequilibrium flux are correct, and that when they are removed from our calculated total disequilibrium flux, the remaining timeseries is a realistic, quasi-top-down terrestrial disequilibrium flux.

When bottom-up ocean disequilibrium fluxes are removed from our calculated total disequilibrium flux, the resulting terrestrial disequilibrium fluxes are, on average for 1991–2007, 30.6 and 22.7 PgC‰ yr$^{-1}$, with 1$\sigma$ residual standard deviations of 12.6 and 12.4 PgC‰ yr$^{-1}$ (after detrending to remove the Suess Effect, as described earlier), when calculated using the Le Quéré et al. (2007) and Park et al. (2010) ocean fluxes, respectively.

We assume an average respiration flux, $F_{ba}$, of 50 PgC yr$^{-1}$, for the length of the record (1991–2007), which is close to the value derived from the CASA response functions. This yields an average isodisequilibrium forcing coefficient, $(\delta_{ba}-\delta_{ab})$, of 0.45‰ when the Park et al. (2010) ocean fluxes are used, and 0.61‰ when the Le Quéré et al. (2007) ocean fluxes are used. Although we do not focus on the magnitude of either the land disequilibrium flux or its forcing coefficient, it is useful to note that our calculated values of $(\delta_{ba}-\delta_{ab})$ fall within the ranges estimated by both bottom-up terrestrial carbon models and atmospheric inversions. For comparison with other results, we extend our linear regression to 1988 and find $(\delta_{ba}-\delta_{ab})$ of 0.40‰ from Park et al. (2010) and 0.48‰ from Le Quéré et al (2007) for that year. Joos and Bruno (1998) calculate an isodisequilibrium forcing coefficient of 0.43‰ for that year. Fung et al. (1997) calculate 0.33‰ in 1988, using a bottom-up terrestrial model, and Scholze et al. (2008) calculate 0.42‰ in 1988, in a model run that takes into account land use changes, $C_4$ crops and $C_4$ pastures. Morimoto et al. (2000) calculate 0.49‰ in 1988, using atmospheric $CO_2$ and $^{13}CO_2$ measurements and an inverse atmospheric transport model.

Re-examination of the constituents of terrestrial disequilibrium flux (eq. 4a) yields insight into potential drivers of high year-to-year variability. First, changes in $\delta_{ab}$ (the $\delta^{13}$C value of

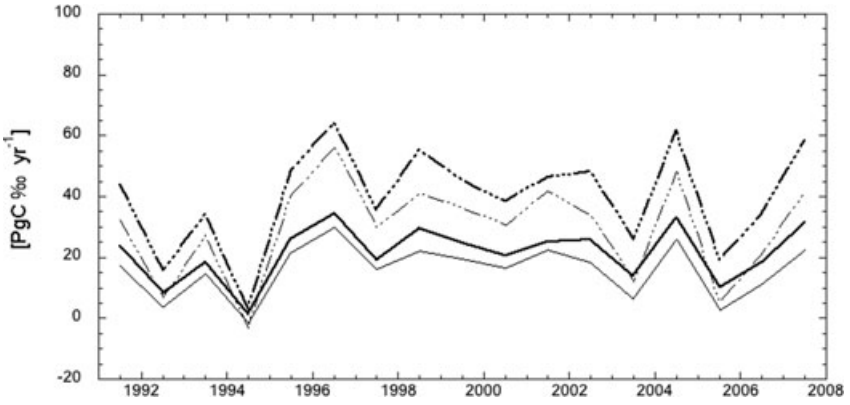


*Fig. 7.* Total global annual mean terrestrial disequilibrium flux, as calculated in the disequilibrium deconvolution using different respiration fluxes. Disequilibrium flux results (Fig. 6), using Park et al. (2010) ocean fluxes (solid lines) and Le Quéré et al. (2007) ocean fluxes (dash-dotted lines), are first adjusted for the bottom-up oceanic component of disequilibrium flux to isolate the terrestrial disequilibrium flux, before being divided by 50 PgC yr$^{-1}$ to isolate ($\delta_{ba}-\delta_{ab}$), which is subsequently multiplied by $F_{ba} = 65$ PgC yr$^{-1}$ (bold lines) and $F_{ba} = 35$ PgC yr$^{-1}$ (fine lines).

newly formed plant matter) can change land disequilibrium flux, without any other changes in eq. 4a. $\delta_{ab}$ is the sum of the $\delta^{13}$C of the atmosphere, which is measured, and discrimination by the terrestrial biosphere during photosynthesis (eq. 3). Changes in plant stomatal opening in response to environmental conditions, and shifts in the proportion of net ecosystem exchange by $C_3$ and $C_4$ plants can, for example, cause discrimination to vary. We discuss these mechanisms and their potential to drive interannual variability in atmospheric $^{13}CO_2$ in Sections 3.5.1 and 3.5.2.

A second possible source of interannual variability in terrestrial disequilibrium flux is $F_{ba}$, the release of carbon from the biosphere by respiration and fire (eq. 4a). It takes time for carbon to move through various biospheric pools before being oxidized by decomposition or combustion, so $F_{ba}$ can be different (aged) enough to reflect significant atmospheric changes due to the Suess Effect. Therefore, a greater release of older, isotopically enriched carbon would cause an increase in total terrestrial disequilibrium flux.

We perform a simple test of the sensitivity of terrestrial disequilibrium flux to changes in $F_{ba}$. Total disequilibrium flux is calculated via the disequilibrium deconvolution (eq. 5), and bottom-up ocean disequilibrium flux is removed to isolate the terrestrial disequilibrium flux. The isodisequilibrium forcing coefficient, ($\delta_{ba}-\delta_{ab}$), is solved for by dividing $D_1$ by 50 PgC yr$^{-1}$ in eq. 4a. ($\delta_{ba}-\delta_{ab}$) is then multiplied by a wide range of $F_{ba}$ values. Terrestrial disequilibrium flux, as calculated with a high ($F_{ba} = 65$ PgC yr$^{-1}$) and a low ($F_{ba} = 35$ PgC yr$^{-1}$) value, is shown in Fig. 7. A significant difference in terrestrial disequilibrium flux is found between these two extremes. Within the envelope of possible respiration flux values, the difference in terrestrial disequilibrium flux ranges from ~5 to 35 PgC‰ yr$^{-1}$. A stepwise increase in respiration results in a slight increase in the magnitude of interannual variability in terrestrial disequilibrium flux, but interannual variability is not greatly altered. However, were heterotrophic respiration to vary widely from year to year, the interannual variability of terrestrial disequilibrium flux would also vary, to the extent that a roughly 85% change in $F_{ba}$ could induce a similar change in terrestrial disequilibrium flux.

In addition to variable rates of heterotrophic respiration, disturbances, especially biomass burning, can change $F_{ba}$. However, the direct effects of biomass burning on terrestrial disequilibrium flux due to changes in respiration flux alone are relatively small. Van der Werf et al. (2006) found that from 1997 to 2004, biomass burning resulted in an average release of $CO_2$ to the atmosphere of 2.5 PgC yr$^{-1}$. They found that interannual variability in $F_{ba}$ from burning was 0.38 PgC yr$^{-1}$ (1$\sigma$ standard deviation) from 1997 to 2004. The largest anomaly occurred during 1998, a strong El Niño year, when biomass burning released 3.7 PgC. If we assume an average respiration flux, $F_{ba}$, of 50 PgC yr$^{-1}$, and an average isodisequilibrium forcing coefficient, ($\delta_{ba}-\delta_{ab}$), of 0.53‰ yr$^{-1}$ (the average of our findings, see Section 3.2), then even the maximum deviation recorded during Van der Werf et al.'s (2006) record would produce a positive terrestrial disequilibrium flux anomaly of only 0.37 PgC‰. Such an anomaly would account for less than 3% of the interannual variability that we calculate in terrestrial disequilibrium flux from 1991 to 2007. Although the contribution of fires to terrestrial disequilibrium flux variability via $F_{ba}$ is small, the degree to which $F_{ba}$ can modulate terrestrial disequilibrium flux by way of anomalies in the $\delta_{ba}$ signature of the vegetation burned can have a large impact on atmospheric $^{13}CO_2$. This source of variability will be discussed later.

A third factor that could, at least mathematically in eq. 4(a), drive disequilibrium flux variability is the residence time of carbon in the terrestrial biosphere. Because the atmosphere is being continuously depleted, changes in the biospheric residence time would augment or diminish the difference between $\delta_{ba}$ and $\delta_{ab}$ (Scholze et al., 2008). To test how much the mean biospheric residence time ($\tau$) would have to change in order to drive all of the variability that we calculate in disequilibrium flux, we can use the simple expression developed by Tans et al. (1993)

$$\delta_{ba} - \delta_{ab} \approx \left(-\frac{d\delta_a}{dt}\right)\tau. \quad (6)$$

Using eq. 4(a) and assuming a constant heterotrophic respiration rate of 50 PgC yr$^{-1}$, we can calculate ($\delta_{ba}-\delta_{ab}$) for 1991 to 2007. During this time period, the growth rate of atmospheric $\delta^{13}$C was

on average about $-0.025‰$, globally. Solving for $\tau$ with these parameters in eq. (6) generates a globally averaged residence time of carbon in the terrestrial biosphere that is more variable than would be believed based upon our current understanding of biospheric carbon sequestration processes. Annual mean residence times generated as described, using the Le Quéré et al. (2007) and the Park et al. (2010) ocean fluxes, would have a $1\sigma$ standard deviation of $\sim$10 years.

The biospheric residence time of carbon is an integration of the mean amount of time it takes for carbon to be cycled through a complex series of pools, or the time elapsed between plant assimilation and oxidation by fire or respiration (Ciais et al., 1999). Changes in residence time can occur from land use changes, but the effects on atmospheric $^{13}CO_2$ are likely smoothed over time, rather than imposing year-to-year anomalies (Scholze et al., 2008). Sudden land use changes (e.g. conversion of a forest to pasture land) and major disturbances (e.g. fires and hurricanes) affect biospheric residence time, but anomalies on the time scale of seasons to years are more appropriately expressed in either $F_{ba}$ or $\delta_{ba}$, rather than in $\tau$ (Ciais et al., 1999). A plausible mechanism by which the residence time of carbon in the biosphere could shift so dramatically from year to year is lacking. We therefore find it highly unlikely that biospheric residence times have the capacity to contribute in any significant way to the interannual variability that we calculate in terrestrial disequilibrium flux.

A fourth potential source of variability in terrestrial disequilibrium flux is $\delta_{ba}$, the $\delta^{13}C$ value of respired carbon. This parameter is connected to variability in residence times of carbon in the biosphere, because multiple pools of carbon, with different rates of carbon cycling, act to homogenize carbon and its isotopic signature before it leaves the biosphere via heterotrophic respiration. Despite interannual variability in fractionation during assimilation of $CO_2$, such oscillations will be dampened by the large reservoir size of the live biomass and soil carbon pools. Therefore, in the absence of respiration flux anomalies, the $\delta^{13}C$ signature of respired material should change smoothly through time.

Anomalies in the $\delta^{13}C$ signature of respired carbon due to disturbances can, however, contribute substantially to atmospheric $^{13}CO_2$ anomalies. Randerson et al. (2005) found that $C_4$ vegetation accounted for 31% of global ecosystem carbon losses from fire in 1997 to 2001, but that burning in forested areas and peatlands (dominated by $C_3$ vegetation) contributed a disproportionately greater amount to atmospheric $^{13}CO_2$ variability. Generally, the burning of $C_4$ vegetation does not have as potent an effect on atmospheric $^{13}CO_2$ as the burning of $C_3$ biomass for two reasons. First, $C_4$ plants fractionate against $^{13}C$ to a lesser extent than $C_3$ plants, so that $C_4$ biomass is closer to the atmospheric $\delta^{13}C$ value than is $C_3$ biomass (O'Leary, 1988). Secondly, about 23% of global $C_4$ aboveground biomass was returned to the atmosphere each year due to biomass burning from 1997 to 2001 (Randerson et al., 2005). The fast turnover time and consequently shorter residence time of carbon in $C_4$ dominated ecosystems, combined with the heavier isotopic signature of $C_4$ biomass, suggest that $C_4$ fire anomalies are less likely to drive large interannual variability in $^{13}CO_2$ than are $C_3$ fire anomalies (Scholze et al., 2008).

Randerson et al. (2005) showed that $C_3$ fire anomalies might have significantly affected interannual variability in atmospheric $^{13}CO_2$ from 1997 to 2001. The time period of their study of $C_3$ and $C_4$ ecosystems spanned both a very strong El Niño event (1997–1998), generally associated with dry conditions and droughts in the tropics, and a La Niña event (2000), generally associated with increased tropical precipitation. They found that the 1997/1998 El Niño was, in fact, the period in which the greatest percent of tropical forests were susceptible to ignition and burning from 1981 to 2001. According to table 1 of Randerson et al. (2005), in 1997 the $\delta^{13}C$ of fire emissions was $-23.5‰$, as compared to a mean value of $-22.9‰$ for 1997–2001. This negative excursion in $\delta_{ba}$ of biomass burning, attributed to an anomalous shift to combustion of more $C_3$ vegetation than usual, could have contributed to a spike in the terrestrial disequilibrium flux of $\sim$2.1 PgC‰ yr$^{-1}$, if multiplied by the total fire emissions during that year (3.5 PgC). An anomaly of this magnitude represents roughly 17% of the variability that we calculate in terrestrial disequilibrium flux. Therefore, in strong fire years (e.g. the 1997/1998 El Niño) and in anomalously moist years during which fires are suppressed (e.g. the La Niña that followed in 2000) shifts in the composition of biomass burning can cause significant terrestrial disequilibrium flux anomalies.

Land use and land cover change can also impact $^{13}CO_2$ fluxes between the terrestrial biosphere and the atmosphere, particularly due to the different degrees to which $C_3$ and $C_4$ vegetation fractionate against $^{13}CO_2$ upon uptake, and to the lag in the $\delta^{13}C$ of respired soil carbon after land use or land cover conversion has occurred (Ciais et al., 1999; Townsend et al., 2002; Scholze et al., 2008). In a recent modelling study, Scholze et al. (2008) quantified the effects of temporal and spatial variability in land use and land cover, with the explicit inclusion of $C_4$ croplands, and pastures. They found that, while the inclusion of this variability in model runs had a significant impact on the average magnitude of global flux-weighted discrimination, it had little to no effect on the interannual variability in discrimination (Fig. 6 in Scholze et al., 2008).

*3.5.1. Discrimination as the source of residual isotopic variability*. In this study, we focus on the possibility that interannual variability in global flux-weighted terrestrial discrimination, which is denoted $\varepsilon_{ab}$ in eq. (3), is the primary driver of residual isotopic variability, and therefore of interannual variability in terrestrial disequilibrium flux. We have shown, in Section 3.5, that variability in $F_{ba}$ and disturbance driven $\delta_{ba}$ anomalies can contribute to residual isotopic variability and to disequilibrium flux variability. Disturbances and respiration flux variability cannot, however, explain all of the variance in terrestrial

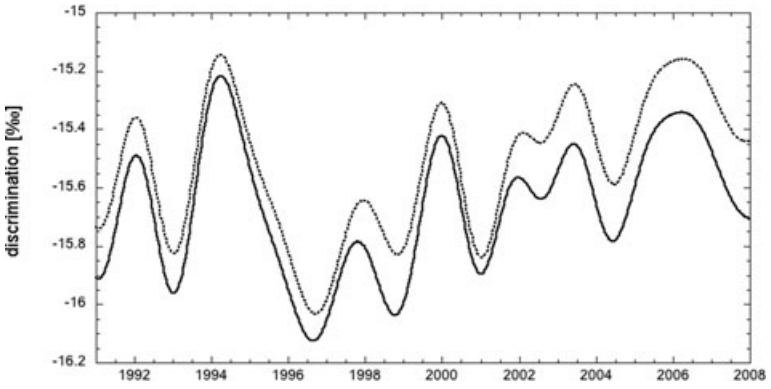


*Fig. 8.* Global mean flux weighted terrestrial discrimination calculated using terrestrial disequilibrium flux from the disequilibrium deconvolution and eqs. (3) and (4a). Calculated with ocean fluxes from Le Quéré et al. (2007) (solid line) and Park et al. (2010) (dotted line).

disequilibrium flux. We therefore consider the extent to which interannual variability in global flux-weighted discrimination can drive terrestrial disequilibrium variability, and whether discrimination variability alone might be sufficient to explain the difference in calculated net air–sea $CO_2$ fluxes between the double deconvolution and the empirical and modelled ocean fluxes.

In Section 2.4, we discussed the historical treatment of discrimination in studies using $\delta^{13}CO_2$ as a carbon cycle tracer. This factor was not typically allowed to vary through time in traditional double deconvolution studies (Keeling et al., 1989, 1995; Quay et al., 1992; Enting et al., 1993, 1995; Tans et al., 1993; Ciais et al., 1995, Francey et al., 1995). Randerson et al. (2002) invoked irregular discrimination as a way to reconcile differences in variability between isotopic and non-isotopic calculations of land and ocean fluxes. The difference between our study and theirs is that they prescribed disequilibrium flux, and allowed discrimination to co-vary with gross primary productivity (GPP) within the double deconvolution framework, whereas we use a different set of constraints to calculate disequilibrium flux, and derive discrimination variability from that solution.

Using eq. 4(a), we force all of the residual isotopic variability into interannual shifts in global mean $\varepsilon_{ab}$ (using the assumptions described in Section 3.2), and find that relatively modest year-to-year shifts in total flux-weighted discrimination (Fig. 8) can satisfy this end-member scenario. The $1\sigma$ standard deviation of the annual mean flux-weighted discrimination that we calculate for 1991–2007 is 0.25‰ $yr^{-1}$ when the Le Quéré et al. (2007) ocean fluxes are used, and 0.26‰ $yr^{-1}$ when the Park et al. (2010) fluxes are used. Randerson et al. (2002) found that reasonable levels of variability in $C_3$ discrimination, and the consequent introduction of a high-frequency component to disequilibrium flux, are capable of attenuating the interannual variability in $F_o$ enough to close the $^{13}CO_2$ budget. We find that reasonable levels of discrimination variability, with both $C_3$ and $C_4$ contributions included, can accommodate both the observed variability in atmospheric $^{13}CO_2$ and the variability of land and ocean sinks expected from bottom-up calculations. The range of interannual variability in discrimination necessary to explain the variability we calculate in our 'top-down' terrestrial disequilibrium flux is higher than that found by Scholze et al. (2003, 2008), who estimated (using a terrestrial model) maximum year to year changes in leaf-level discrimination (including the contributions of both $C_3$ and $C_4$ vegetation) of roughly 0.3‰ $yr^{-1}$ (i.e. a full range of ±0.15‰ $yr^{-1}$ and standard deviation significantly less than that).

*3.5.2. Drivers of discrimination variability.* If we are to invoke changing discrimination as a mechanism for disequilibrium flux variability, then we must investigate plausible drivers of such year-to-year oscillations. $C_3$ plant discrimination has been shown by both observations and models to vary widely in response to climate variability (Bowling et al., 2002; Ometto et al., 2002; Pataki et al., 2003), as plants open and close their stomata to optimize internal $CO_2$ concentrations while minimizing transpiration (Farquhar et al., 1982). Scholze et al. (2003) found that process-based model simulations produced 5 PgC‰ $yr^{-1}$ more interannual variability in terrestrial disequilibrium flux when discrimination was allowed to vary only in response to climate (their 'ISOVAR' run), as opposed to fixed discrimination (their 'ISOFIX' run).

Discrimination can also vary as a result of shifts in the proportion of net ecosystem exchange (NEE) by $C_3$ and $C_4$ plants (Kaplan et al., 2002). $C_4$ plants fractionate less against $^{13}C$ because $CO_2$ is fixed by the non-fractionating and irreversible step of carboxylation by phosphoenolpyruvate, prior to carboxylation by ribulose biphosphate (O'Leary, 1988; Farquhar et al., 1989). Shifts towards more $C_3$ ($\varepsilon_{ab} \approx -18‰$) than $C_4$ ($\varepsilon_{ab} \approx -4‰$) exchange would lead to higher flux-weighted discrimination and vice versa. $C_4$-dominated ecosystems, as well as ecosystems with mixes of $C_3$ and $C_4$ vegetation, have been shown to have very high year-to-year variability in carbon cycling in response to temperature and precipitation changes (Knapp and Smith, 2001; Suyker et al., 2003). Consequently, high variability in total isotopic discrimination of such systems has been documented (Still et al., 2003). At the global scale of our calculations, the biosphere is a mixed $C_3/C_4$ system, where productivity changes within $C_3$ and $C_4$ biomes could lead to changing flux-weighted global values of $\varepsilon_{ab}$.

We investigate how variable the ratio of $C_4$ to total NEE would need to be, to absorb all residual isotopic variability and therefore to explain all of the interannual variability in our 'top-down' terrestrial disequilibrium flux. We use the following equation to deconvolve $\varepsilon_{ab}$, as calculated in Section 3.2, into a timeseries of the relative contributions of $C_3$ and $C_4$ vegetation to global NEE

$$\varepsilon_{ab} = -4‰ C_4 + -18‰(1 - C_4). \quad (7)$$

Interannual variability in $C_4$ vegetation, as a fraction of NEE, of $\pm 1.8\%$ can explain all of the residual isotopic variability when bottom-up ocean results are combined with atmospheric observations. For 1991–2007, the $1\sigma$ standard deviation of the annual mean fraction that $C_4$ NEE makes up of total ($C_4 + C_3$) NEE is 1.8% when calculated with the Le Quéré et al. (2007) ocean fluxes, and 1.8% when calculated with the Park et al. (2010) ocean fluxes. As yet, there are few independent and no observational estimates of such variability on year-to-year time scales to falsify this hypothesis. Using a dynamic global vegetation model to simulate year-to-year changes in $C_3$ and $C_4$ vegetation, Scholze et al. (2003) calculated a maximum variability of 0.1‰ in $\varepsilon_{ab}$ (in their 'ISOFIX' run). By our calculations, this would result in interannual variability of $\pm 0.7\%$. Scholze et al. (2008) did create timeseries of global $C_4$ pasture, $C_4$ crop, and $C_4$ land use coverage. However, year-to-year variations were based largely on interpolation and extrapolation, especially after 1990, thus diminishing their variability. Moreover, global interannual variability in total $C_3/C_4$ vegetation is not explicitly given in that paper. For the $C_4$ fraction of NEE to explain all of our calculated variability in terrestrial disequilibrium flux would be one end member scenario. The calculated interannual variability of $\pm 1.8\%$ likely represents the maximum limit of variability in the $C_4$ fraction of NEE, as this scenario simultaneously assumes no interannual variability in $C_3$ discrimination.

We calculate interannual variability in discrimination that can be reasonably explained by a combination of $C_3$ discrimination and $C_3/C_4$ vegetation shifts, and that is slightly higher than the findings of Scholze et al. (2003), who use a dynamic global vegetation model. We calculate standard deviation of discrimination of 0.25–0.26‰ $yr^{-1}$ ($1\sigma$) for 1991–2007, and they find that $C_3$ discrimination and $C_3/C_4$ vegetation shifts can cause interannual variability in global leaf-level discrimination of $\sim\pm 0.15$‰, when averaged over 100 years. They attribute $\sim$0.1‰ of this variability (i.e. $\pm 0.05$‰) to shifts in the productivity of $C_3$ and $C_4$ plants. If we assume that, as the Scholze et al. (2003) model suggests, one-third of our calculated discrimination is caused by changes in the $C_4$ fraction of NEE, then this would imply a mean interannual variability in the $C_4$ fraction of $\pm 0.62\%$ $yr^{-1}$ when the Park et al. (2010) ocean fluxes are used and $\pm 0.60\%$ $yr^{-1}$ when the Le Quéré et al. (2007) ocean fluxes are used. The remaining $\pm 0.17$‰ $yr^{-1}$ (from both Le Quéré et al., 2007 and Park et al., 2010) of interannual variability in discrimination would, in that case, be due to changes in $C_3$ discrimination alone. Interannual variability in $C_3$ discrimination of this order fits well with the calculation of Randerson et al. (2002), who found interannual variability in $C_3$ discrimination of $\pm 0.2$‰ when they parameterized discrimination to covary with GPP in a bottom-up biosphere model.

In the absence of direct measures against which to gauge the plausibility of our results, we have tried to correlate our findings to climatic indicators thought to control the geographic distribution, photosynthetic rates, and discrimination of $C_3$ and $C_4$ vegetation. For $C_3$ plants, we expect a positive correlation between precipitation and fractionation, because plant stomata close (thus reducing fractionation) in dry conditions to reduce water loss. However, in $C_4$ grasslands this relationship could be the opposite, given that growing season precipitation is a strong control on $C_4$ photosynthetic rates (Lambers et al., 1998). The relationship between temperature and total fractionation is even less clear. Attempts to correlate temperature, precipitation, and soil moisture anomalies with our global results have so far been unsuccessful, likely because global heterogeneity in these parameters, and in $C_4/C_3$ vegetation variability, as well as in the possible competing impacts of $C_3$ and $C_4$ fractionation, precludes isolation of clear, coherent signals. Future efforts to better understand causes of disequilibrium flux variability will require using models that resolve individual regions of the globe to compare disequilibrium flux and discrimination with climate at finer spatial scales.

### *3.6. Are anti-correlations between land and ocean fluxes real?*

The double deconvolution approach produces estimates for surface ocean $CO_2$ fluxes that are more variable than can be explained by $\Delta pCO_2$-based approaches or ocean models. The land and ocean flux estimates produced by the double deconvolution are also notably anti-correlated (Fig. 5b). Historically, anti-correlations found in double deconvolution results have been treated with caution, as they can be interpreted as a sign of imperfect budgeting techniques rather than of true reservoir variability (Francey et al., 1995; Joos and Bruno, 1998). A similar anti-correlation between ocean and land flux estimates is found when $O_2/N_2$ is used to partition the $CO_2$ sink, and is interpreted with equal suspicion (Bender et al., 2005).

However, we find that when the bottom-up ocean fluxes of Le Quéré et al. (2007) and Park et al. (2010) are magnified, similar temporal patterns of source–sink oscillations to those determined by the double deconvolution method are seen (Fig. 9). Although the scale of variability is different between the two independent approaches, the general phasing is similar. For example, from midway through 1995 to midway through 1997, from 1999 to 2002, from 2004 to 2005 and possibly even from 2007 to 2008 (the bottom-up record ends here), lows in the double deconvolution land flux (which are also seen in other estimates of the land flux, as discussed in Section 3.1) are matched with highs in all three ocean timeseries. Similarly, from 1997 to 1999, and

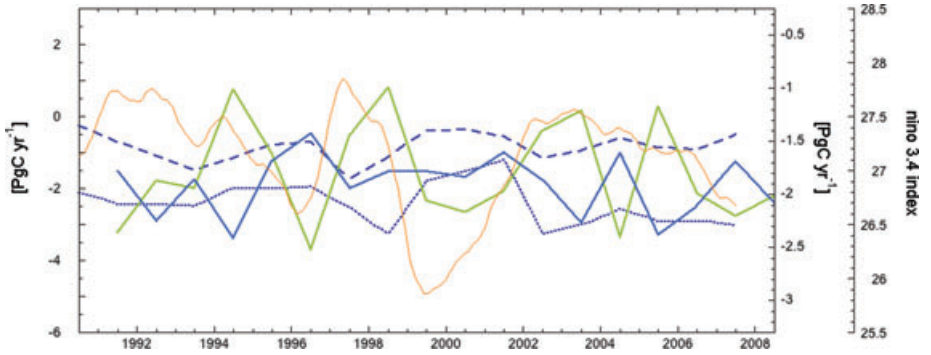


*Fig. 9.* Double deconvolution ocean (solid blue line) and land (green line) fluxes on left *Y*-axis, and bottom-up ocean flux estimates from Le Quéré et al. (2007) (dotted dark blue line) and Park et al. (2010) (dashed dark blue line) on right *Y*-axis; global annual means. To enable direct comparison of phasing, bottom-up ocean estimates are placed on the right axis so that magnitude and variability match that of the double deconvolution ocean flux, which are placed on the left axis. The far right *Y*-axis is for the Nino 3.4 Sea Surface Temperature Index from the NOAA Climate Prediction Center (plotted in orange); 2-year running mean.

from 2002 to 2004, high land fluxes appear to be matched with a low ocean fluxes. This could suggest that the anti-phasing between ocean and land sinks may in fact have a geophysical explanation in some years. However, we caution that a correlation analysis yields low correlation coefficients when the Le Quéré et al. (2007) and Park et al. (2010) annual mean ocean fluxes are compared with the double deconvolution ocean fluxes ($R^2 = 0.10$ and 0.15, respectively). We note that a linear correlation analysis between the Le Quéré et al. (2007) and Park et al. (2010) annual mean ocean fluxes yields a similarly low $R^2$ of 0.18. Small shifts in the baseline value of the three ocean flux timeseries may attenuate the correlations between them.

Comparison of ocean fluxes with a 2-year running mean of the niño 3.4 sea surface temperature index (Fig. 9) suggests a strong anti-correlation with the warm sea surface temperatures in the niño 3.4 region (positive anomalies in which are indicative of El Niño conditions). It is particularly interesting to note that, while the land flux seems to lag the niño 3.4 index, the ocean fluxes display a much shorter lag, if any, in their anti-correlation with the index. These observations agree with many studies showing that interannual variability in the net air–sea $CO_2$ flux is correlated to El Niño Southern Oscillation (ENSO) variability (e.g. Bacastow, 1976; Rayner et al., 1999). Figure 9 further suggests that there are strong physical connections between ENSO and the net terrestrial flux. During El Niño years, such as 1998, tropical drying may cause increased release of carbon through respiration and burning (e.g. van der Werf et al., 2004), while under the same conditions global net ocean uptake may increase due to dampened upwelling (and attenuated local release of $CO_2$) off the coast of South America (Winguth et al., 1994; Chavez et al., 1999).

## 4. Conclusions

We have used atmospheric observations of $CO_2$ and $\delta^{13}C$ with bottom-up net air–sea fluxes to determine interannual variability in global disequilibrium flux. Although the high level of variability in disequilibrium flux is inconsistent with the $^{13}C$ Suess Effect, we find that, taken together, variability in a range of terrestrial isotopic parameters can explain the disequilibrium changes (Fig. 10). We find that reasonable amounts of variability in photosynthetic discrimination ($1\sigma$ standard deviation of 0.25–0.26‰ $yr^{-1}$) can explain the interannual variability that we calculate in terrestrial disequilibrium flux (±12.4–12.6 PgC‰ $yr^{-1}$, average deviations from the trend). Together with bottom-up estimates of air–sea $CO_2$ flux and ocean disequilibrium flux, the observed interannual variability in atmospheric $^{13}CO_2$ can be explained. We therefore conclude that bottom-up estimates for the net air–sea $CO_2$ flux (and ocean disequilibrium flux) can be reconciled with observed isotopic variability in atmospheric $^{13}CO_2$ if that variability is expressed by the terrestrial disequilibrium flux. Although the resulting interannual variability in disequilibrium flux is high, year-to-year shifts in this term can be explained by modest changes in total terrestrial discrimination.

Our calculations are within the range of discrimination variability estimated by bottom-up biosphere models. For example, Scholze et al. (2003) find that discrimination variability can contribute up to 15 PgC‰ $yr^{-1}$ of interannual variability in $^{13}CO_2$ fluxes. Following Scholze et al.'s (2003) partitioning of total leaf-level discrimination into contributions of one-third from $C_3/C_4$ vegetation shifts and of two-thirds from $C_3$ discrimination, we calculate that $C_3$ discrimination can vary interannually by ±0.17‰ $yr^{-1}$. Randerson et al. (2002) estimate interannual variability in $C_3$ discrimination of ±0.2‰.

The above conclusions neglect, however, the likely contributions of variations in biospheric respiration/fire and its $\delta^{13}C$ value to interannual variability in terrestrial disequilibrium flux. In reality, terrestrial disequilibrium flux variability is most likely the result of some combination of $C_3$ stomatal conductance changes in response to water stress, $C_3/C_4$ vegetation shifts, variable rates of biospheric $CO_2$ respiration, and disturbance driven shifts in

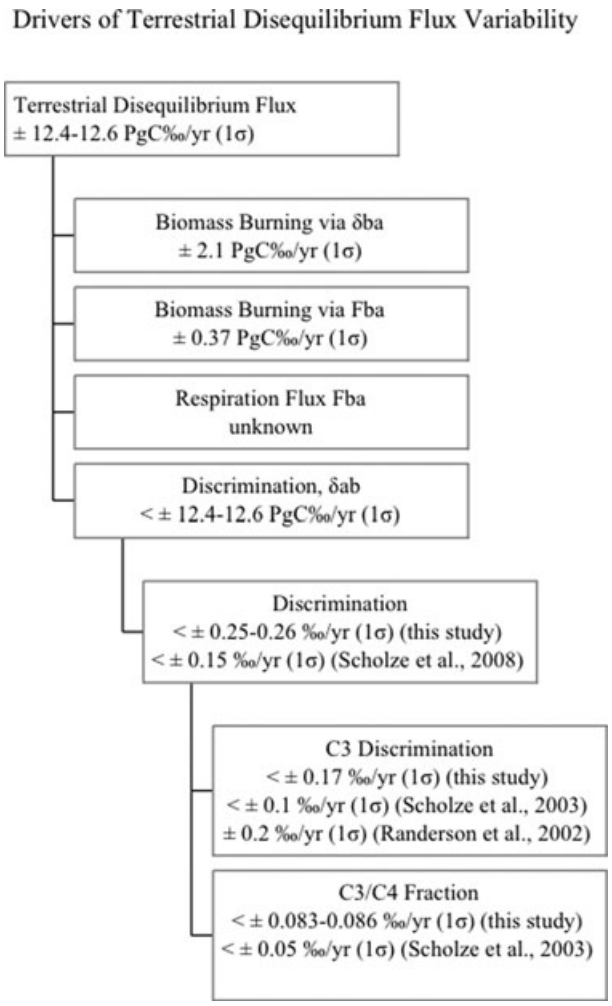


*Fig. 10.* Potential drivers of interannual variability in terrestrial disequilibrium flux are shown with possible magnitudes of variability. Results from this study are compared with other studies, where possible.

$\delta_{ba}$ (Fig. 10). This conclusion is supported by the conclusion that our estimate of total interannual variability in discrimination (±0.25–0.26‰ $yr^{-1}$, 1$\sigma$ standard deviation) is higher than that modelled by Scholze et al. (2008) (less than ±0.15‰). Some component of our calculated discrimination variability is almost certainly actually attributable to $F_{ba}$ and $\delta_{ba}$ variability, and not to discrimination, especially given the fact that our timeseries spans the exceptionally strong El Niño event of 1997/1998.

In addition, we can not rule out that changes in gross ocean–atmosphere fluxes, possibly resulting from widespread windspeed anomalies, could also play a role in leading to a more variable ocean disequilibrium flux than we have modelled. Finally, we cannot rule out the possibility that net ocean fluxes may indeed be more variable than currently believed. It is striking that the process-model based net ocean flux and that estimated from the double deconvolution have very similar phasing, and it may be that the truth lies in a more variable ocean flux than models currently predict, combined with a more variable disequilibrium flux than has been used in past double deconvolutions.

Two parallel avenues of research could justify greatly narrowing the uncertainty in interannual net ocean fluxes: (a) increased confidence in ocean model (e.g. Le Quéré et al., 2007) and empirical $\Delta pCO_2$-based approaches (e.g. Park et al., 2010), and (b) using atmospheric $CO_2$ alone with much greater density of observations over land and oceans (e.g. Peters et al., 2007). This could, to a large extent, obviate the traditional use of $\delta^{13}C$ to partition land and ocean fluxes. A complimentary line of study will be to more carefully examine the origins of $^{13}CO_2$ anomalies in time and space. As the density of atmospheric observations of $CO_2$ and $^{13}CO_2$ continues to increase, the spatial origin of $^{13}CO_2$ anomalies are becoming a crucial proxy for understanding the processes driving $^{13}CO_2$ variability (Langenfelds et al., 2002; Rayner et al., 2008).

Although uncertainty in the magnitude of variability persists, this work nonetheless makes it clear that, if bottom-up estimates of ocean surface exchange correctly identify this flux as having relatively low interannual variability, then the residual isotopic variability must reside elsewhere, and the global isotopic disequilibrium flux may be much more variable than has been previously believed. The analysis shown here demonstrates that knowing ocean fluxes more confidently could allow us to quantify variability in terrestrial disequilibrium flux, its drivers, and the relationships between those mechanisms and environmental variables. As such, it could serve several purposes. A top-down estimation of discrimination would be an important diagnostic tool for variability in the mechanisms driving terrestrial carbon cycling. As an independent means for comparison with bottom-up terrestrial models, it could serve to validate these approaches as well as to identify sources for isotopic variability that bottom-up approaches may miss. In addition, an atmosphere-constrained estimation of disequilibrium flux could serve as a tool for parameterization of disequilibrium flux and discrimination variability in bottom-up models. This would be particularly useful when more meaningful relationships are established between disequilibrium flux and discrimination variability and the suite of climatic indicators thought to influence these terms: temperature, precipitation and vapour pressure deficit, among others.

## 5. Acknowledgments

The authors first thank all of the sample collectors at all of the NOAA/ESRL sampling sites for their dedication and hard work. The authors thank Bruce Vaughn, Sylvia Michel, Amy Steiker and Jason Winokur for the preparation and analysis of $\delta^{13}C$ data, and Patricia Lang, Kelly Sours and Thomas Conway for $CO_2$ analysis and data; Ken Masarie for creating global means and help with figures; Pieter Tans for ocean disequilibrium calculation algorithms; Neil Suits for SiB2 terrestrial fractionation model output; Jim Randerson for providing CASA impulse-response functions; Nikki Lovenduski for discussion

regarding ocean $CO_2$ flux variability; and the valuable input of those who contributed to the review process of this paper. This work was funded in part by the NOAA Climate Program Office.

## References

BP Statistical Review of World Energy June. 2009. www.bp.com/statisticalreview.

Bacastow, R. B. 1976. Modulation of atmospheric carbon-dioxide by southern oscillation. *Nature* **261**, 116–118.

Baker, D. F., Law, R. M., Gurney, K. R., Rayner, P., Peylin, P. and co-authors. 2006. TransCom 3 inversion intercomparison: impact of transport model errors on the interannual variability of regional $CO_2$ fluxes, 1988–2003. *Global Biogeochem. Cycles* **20**, GB1002, doi:10.1029/2004GB002439.

Battle, M., Bender, M. L., Tans, P. P., White, J. W. C., Ellis, J. T. and co-authors. 2000. Global carbon sinks and their variability inferred from atmospheric $O_2$ and delta C-13. *Science* **287**, 2467–2470.

Bender, M. L., Ho, D. T., Hendricks, M. B., Mika, R., Battle, M. O. and co-authors. 2005. Atmospheric $O_2/N_2$ changes, 1993–2002: implications for the partitioning of fossil fuel $CO_2$ sequestration. *Global Biogeochem. Cycles* **19**, GB4017, doi:10.1029/2004GB002410.

Boden, T. A., Marland, G. and Andres, R. J. 2009. Global, regional, and national fossil-fuel $CO_2$ emissions. Carbon Dioxide Information Analysis Center, Oak Ridge National Laboratory, U.S. Department of Energy, Oak Ridge, TN, U.S.A., doi:10.3334/CDIAC/00001.

Bousquet, P., Peylin, P., Ciais, P., Le Quéré, C., Friedlingstein, P. and co-authors. 2000. Regional changes in carbon dioxide fluxes of land and oceans since 1980. *Science* **290**, 1342–1346.

Bowling, D. R., McDowell, N. G., Bond, B. J., Law, B. E. and Ehleringer, J. R. 2002. C-13 content of ecosystem respiration is linked to precipitation and vapor pressure deficit. *Oecologia* **131**, 113–124.

Buitenhuis, E., Le Quéré, C., Aumont, O., Beaugrand, G., Bunker, A. and co-authors. 2006. Biogeochemical fluxes through mesozooplankton. *Global Biogeochem. Cycles* **20**, GB2003, doi:10.1029/2005GB002511.

Canadell, J. G., Le Quéré, C., Raupach, M. R., Field, C. B., Buitenhuis, E. T. and co-authors. 2007. Contributions to accelerating atmospheric $CO_2$ growth from economic activity, carbon intensity, and efficiency of natural sinks. *Proc. Natl. Acad. Sci. USA* **104**, 18866–18870.

Chavez, F. P., Strutton, P. G., Friederich, C. E., Feely, R. A., Feldman, G. C. and co-authors. 1999. Biological and chemical response of the equatorial Pacific Ocean to the 1997–98 El Niño. *Science* **286**, 2126–2131.

Ciais, P., Tans, P. P., White, J. W. C., Trolier, M., Francey, R. J. and co-authors. 1995. Partitioning of ocean and land uptake of $CO_2$ as inferred by delta C-13 measurements from the NOAA climate monitoring and diagnostics laboratory global air sampling network. *J. Geophys. Res.-Atmos.* **100**, 5051–5070.

Ciais, P., Friedlingstein, P., Schimel, D. S. and Tans, P. P. 1999. A global calculation of the delta C-13 of soil respired carbon: implications for the biospheric uptake of anthropogenic CO2. *Global Biogeochem. Cycles* **13**, 519–530.

Collatz, G. J., Ball, J. T., Grivet, C. and Berry, J. A. 1991. Physiological and environmental-regulation of stomatal conductance, photosynthesis and transpiration – a model that includes a laminar boundary-layer. *Agric. Forest Meteorol.* **54**, 107–136.

Conway, T. J., Tans, P. P., Waterman, L. S. and Thoning, K. W. 1994. Evidence for interannual variability of the carbon-cycle from the national-oceanic-and-atmospheric-administration climate-monitoring-and-diagnostics-laboratory global-air-sampling-network. *J. Geophys. Res.-Atmos.* **99**, 22831–22855.

DeFries, R. S., Houghton, R. A., Hansen, M. C., Field, C. B., Skole, D. and co-authors. 2002. Carbon emissions from tropical deforestation and regrowth based on satellite observations for the 1980s and 1990s. *Proc. Natl. Acad. Sci. USA* **99**, 14256–14261.

Denman, K. L., Brasseur, G., Chidthaisong, A., Ciais, P., Cox, P. M. and co-authors. 2007. Couplings between changes in the climate system and biogeochemistry. In: *Climate Change 2007: The Physical Science Basis. Contribution of Working Group I to the Fourth Assessment report of the Intergovernmental Panel on Climate Change* (eds S., Solomon, D., Qin, M., Manning, Z., Chen, M., Marquis, and co-authors). Cambridge, United Kingdom, New York, NY, USA, 500–587.

Doney, S. C., Tilbrook, B., Roy, S., Metzl, N., Le Quéré, C. and co-authors. 2009a. Surface-ocean $CO_2$ variability and vulnerability. *Deep-Sea Res. Part II-Topical Stud. Oceanogr.* **56**, 504–511.

Doney, S. C., Lima, I., Feely, R. A., Glover, D. M., Lindsay, K. and co-authors. 2009b. Mechanisms governing interannual variability in upper-ocean inorganic carbon system and air-sea $CO_2$ fluxes: physical climate and atmospheric dust. *Deep-Sea Res. Part II-Topical Stud. Oceanogr.* **56**, 640–655.

Enting, I. G., Trudinger, C. M., Francey, R. J. and Granek, H. 1993. Synthesis inversion of atmospheric $CO_2$ using the GISS tracer transport model. *Aust. Div. Atmos. Res. Tech. Pap.* **29**, 1–44.

Enting, I. G., Trudinger, C. M. and Francey, R. J. 1995. A synthesis inversion of the concentration and delta C-13 of atmospheric $CO_2$. *Tellus* **47B**, 35–52.

Etheridge, D. M., Steele, L. P., Langenfelds, R. L., Francey, R. J., Barnola, J. M. and co-authors. 1996. Natural and anthropogenic changes in atmospheric $CO_2$ over the last 1000 years from air in Antarctic ice and firn. *J. Geophys. Res.-Atmos.* **101**, 4115–4128.

Farquhar, G. D., Oleary, M. H. and Berry, J. A. 1982. On the relationship between carbon isotope discrimination and the inter-cellular carbon-dioxide concentration in leaves. *Aust. J. Plant Physiol.* **9**, 121–137.

Farquhar, G. D., Ehleringer, J. R. and Hubick, K. T. 1989. Carbon isotope discrimination and photosynthesis. *Ann. Rev. Plant Physiol. Plant Molec. Biol.* **40**, 503–537.

Francey, R. J. 1985. Cape grim isotope measurements – a preliminary assessment. *J. Atmos. Chem.* **3**, 247–260.

Francey, R. J., Tans, P. P., Allison, C. E., Enting, I. G., White, J. W. C. and co-authors. 1995. Changes in oceanic and terrestrial carbon uptake since 1982. *Nature* **373**, 326–330.

Francey, R. J., Allison, C. E., Etheridge, D. M., Trudinger, C. M., Enting, I. G. and co-authors. 1999. A 1000-year high precision record of delta C-13 in atmospheric $CO_2$. *Tellus* **51B**, 170–193.

Fung, I., Field, C. B., Berry, J. A., Thompson, M. V., Randerson, J. T. and co-authors. 1997. Carbon 13 exchanges between the atmosphere and biosphere. *Global Biogeochem. Cycles* **11**, 507–533.

Gruber, N., Keeling, C. D., Bacastow, R. B., Guenther, P. R., Lueker, T. J. and co-authors. 1999. Spatiotemporal patterns of carbon-13 in the global surface oceans and the oceanic Suess Effect. *Global Biogeochem. Cycles* **13**, 307–335.

Houghton, R. A. 2003. Revised estimates of the annual net flux of carbon to the atmosphere from changes in land use and land management 1850–2000. *Tellus* **55B**, 378–390.

Joos, F. and Bruno, M. 1998. Long-term variability of the terrestrial and oceanic carbon sinks and the budgets of the carbon isotopes C-13 and C-14. *Global Biogeochem. Cycles* **12**, 277–295.

Kaplan, J. O., Prentice, I. C. and Buchmann, N. 2002. The stable carbon isotope composition of the terrestrial biosphere: modeling at scales from the leaf to the globe. *Global Biogeochem. Cycles* **16**, 1060–1071.

Keeling, C. D. 1960. The concentration and isotopic abundances of carbon dioxide in the atmosphere. *Tellus* **12**, 200–203.

Keeling, C. D. 1979. The Suess Effect: $^{13}$Carbon-$^{14}$Carbon interrelations. *Environ. Int.* **2**, 229–300.

Keeling, C. D., Bastacow, R. B., Carter, A. F., Piper, S. C., Whorf, T. P. and co-authors. 1989. A three-dimensional model of atmospheric $CO_2$ transport based on observed winds: analysis of observational data. In: *Aspects of climate variability in the Pacific and the Western Americas* (ed. D. H., Peterson). American Geophysical Union, Washington, DC, 165–236.

Keeling, C. D., Whorf, T. P., Wahlen, M. and Vanderplicht, J. 1995. Interannual extremes in the rate of rise of atmospheric carbon dioxide since 1980. *Nature* **375**, 666–670.

Knapp, A. K. and Smith, M. D. 2001. Variation among biomes in temporal dynamics of aboveground primary production. *Science* **291**, 481–484.

Krakauer, N. Y., Randerson, J. T., Primeau, F. W., Gruber, N. and Menemenlis, D. 2006. Carbon isotope evidence for the latitudinal distribution and wind speed dependence of the air-sea gas transfer velocity. *Tellus* **58B**, 390–417.

Lambers, H., Chapin, F. S. and Pons, T. L. 1998. *Plant Physiological Ecology*. Springer, New York, 70–71.

Langenfelds, R. L., Francey, R. J., Pak, B. C., Steele, L. P., Lloyd, J. and co-authors. 2002. Interannual growth rate variations of atmospheric $CO_2$ and its delta C-13, $H_2$, $CH_4$, and CO between 1992 and 1999 linked to biomass burning. *Global Biogeochem. Cycles* **16**, 1048–1069.

Le Quéré, C., Aumont, O., Bopp, L., Bousquet, P., Ciais, P. and co-authors. 2003. Two decades of ocean CO2 sink and variability. *Tellus* **55B**, 649–656.

Le Quéré, C., Rödenbeck, C., Buitenhuis, E. T., Conway, T. J., Langenfelds, R. and co-authors. 2007. Saturation of the Southern Ocean $CO_2$ sink due to recent climate change. *Science* **316**, 1735–1738.

Le Quéré, C., Raupach, M. R., Canadell, J. G., Marland, G., Bopp, L. and co-authors. 2009. Trends in the sources and sinks of carbon dioxide. *Nature Geosci.* **2**, 831–836.

Lee, K., Wanninkhof, R., Takahashi, T., Doney, S. C. and Feely, R. A. 1998. Low interannual variability in recent oceanic uptake of atmospheric carbon dioxide. *Nature* **396**, 155–159.

Lloyd, J. and Farquhar, G. D. 1994. C-13 discrimination during $CO_2$ assimilation by the terrestrial biosphere. *Oecologia* **99**, 201–215.

Masarie, K. A. and Tans, P. P. 1995. Extension and integration of atmospheric carbon-dioxide data into a globally consistent measurement record. *J. Geophys. Res.-Atmos.* **100**, 11593–11610.

Matsumoto, K., Sarmiento, J. L., Key, R. M., Aumont, O., Bullister, J. L. and co-authors. 2004. Evaluation of ocean carbon cycle models with data-based metrics. *Geophys. Res. Lett.* **31**, L07303, doi:10.1029/2003GL018970.

Morimoto, S., Nakazawa, T., Higuchi, K. and Aoki, S. 2000. Latitudinal distribution of atmospheric $CO_2$ sources and sinks inferred by delta C-13 measurements from 1985 to 1991. *J. Geophys. Res.-Atmos.* **105**, 24315–24326.

Naegler, T., Ciais, P., Rodgers, K. and Levin, I. 2006. Excess radiocarbon constraints on air-sea gas exchange and the uptake of $CO_2$ by the oceans. *Geophys. Res. Lett.* **33**, L11802, doi:10.1029/2005GL025408.

O'leary, M. H. 1988. Carbon isotopes in photosynthesis. *Bioscience* **38**, 328–336.

Obata, A. and Kitamura, Y. 2003. Interannual variability of the sea-air exchange of $CO_2$ from 1961 to 1998 simulated with a global ocean circulation-biogeochemistry model. *J. Geophys. Res.-Oceans* **108**, 3337–3351.

Olsen, A., Wanninkhof, R., Trinanes, J. A. and Johannessen, T. 2005. The effect of wind speed products and wind speed-gas exchange relationships on interannual variability of the air-sea $CO_2$ gas transfer velocity. *Tellus* **57B**, 95–106.

Ometto, J., Flanagan, L. B., Martinelli, L. A., Moreira, M. Z., Higuchi, N. and co-authors. 2002. Carbon isotope discrimination in forest and pasture ecosystems of the Amazon Basin, Brazil. *Global Biogeochem. Cycles* **16**, 1109–1118.

Orr, J. C., Maier-Reimer, E., Mikolajewicz, U., Monfray, P., Sarmiento, J. L. and co-authors. 2001. Estimates of anthropogenic carbon uptake from four three-dimensional global ocean models. *Global Biogeochem. Cycles* **15**, 43–60.

Page, S. E., Siegert, F., Rieley, J. O., Boehm, H. D. V., Jaya, A. and co-authors. 2002. The amount of carbon released from peat and forest fires in Indonesia during 1997. *Nature* **420**, 61–65.

Park, G. H., Lee, K., Wanninkhof, R. and Feely, R. A. 2006. Empirical temperature-based estimates of variability in the oceanic uptake of $CO_2$ over the past 2 decades. *J. Geophys. Res.-Oceans* **111**, C07S07, doi:10.1029/2005JC003090.

Park, G. H., Wanninkhof, R., Doney, S. C., Takahashi, T., Lee, K. and co-authors. 2010. Variability of the global net sea-air $CO_2$ fluxes over the last three decades using empirical relationships. *Tellus B*, doi:10.1111/j.1600-0889.2010.00498.x.

Pataki, D. E., Ehleringer, J. R., Flanagan, L. B., Yakir, D., Bowling, D. R. and co-authors. 2003. The application and interpretation of Keeling plots in terrestrial carbon cycle research. *Global Biogeochem. Cycles* **17**, 1022–1035.

Peters, W., Jacobson, A. R., Sweeney, C., Andrews, A. E., Conway, T. J. and co-authors. 2007. An atmospheric perspective on North American carbon dioxide exchange: CarbonTracker. *Proc. Natl. Acad. Sci. USA* **104**, 18925–18930.

Quay, P. D., Tilbrook, B. and Wong, C. S. 1992. Oceanic uptake of fossil-fuel $CO_2$—C-13 evidence. *Science* **256**, 74–79.

Randerson, J. T., Collatz, G. J., Fessenden, J. E., Munoz, A. D., Still, C. J. and co-authors. 2002. A possible global covariance between terrestrial gross primary production and C-13 discrimination: consequences for the atmospheric C-13 budget and its response to ENSO. *Global Biogeochem. Cycles* **16**, 1136–1151.

Randerson, J. T., Van Der Werf, G. R., Collatz, G. J., Giglio, L., Still, C. J. and co-authors. 2005. Fire emissions from C-3 and C-4 vegetation and their influence on interannual variability of atmospheric

$CO_2$ and delta(CO2)-C-13. *Global Biogeochem. Cycles* **19**, GB2019, doi:10.1029/2004GB002366.

Rayner, P. J., Law, R. M. and Dargaville, R. 1999. The relationship between tropical CO2 fluxes and the El Niño -Southern Oscillation. *Geophys. Res. Lett.* **26**, 493–496.

Rayner, P. J., Law, R. M., Allison, C. E., Francey, R. J., Trudinger, C. M. and co-authors. 2008. Interannual variability of the global carbon cycle (1992–2005) inferred by inversion of atmospheric $CO_2$ and $\delta^{13}CO_2$ measurements. *Global Biogeochem. Cycles* **22**, GB3008, doi:10.1029/2007GB003068.

Rödenbeck, C., Houweling, S., Gloor, M. and Heimann, M. 2003. $CO_2$ flux history 1982–2001 inferred from atmospheric data using a global inversion of atmospheric transport. *Atmos. Chem. Phy.* **3**, 1919–1964.

Scholze, M., Kaplan, J. O., Knorr, W. and Heimann, M. 2003. Climate and interannual variability of the atmosphere-biosphere $^{13}CO_2$ flux. *Geophys. Res. Lett.* **30**, 1097–1101.

Scholze, M., Ciais, P. and Heimann, M. 2008. Modeling terrestrial C-13 cycling: climate, land use and fire. *Global Biogeochem. Cycles* **22**, GB1009, doi:10.1029/2006GB002899.

Siegenthaler, U. and Oeschger, H. 1987. Biospheric $CO_2$ emissions during the past 200 years reconstructed by deconvolution of ice core data. *Tellus* **39B**, 140–154.

Still, C. J., Berry, J. A., Collatz, G. J. and DeFries, R. S. 2003. Global distribution of C-3 and C-4 vegetation: carbon cycle implications. *Global Biogeochem. Cycles* **17**, 1006–1019.

Suits, N. S., Denning, A. S., Berry, J. A., Still, C. J., Kaduk, J. and co-authors. 2005. Simulation of carbon isotope discrimination of the terrestrial biosphere. *Global Biogeochem. Cycles* **19**, GB1017, doi:10.1029/2003GB002141.

Suyker, A. E., Verma, S. B. and Burba, G. G. 2003. Interannual variability in net $CO_2$ exchange of a native tallgrass prairie. *Global Change Biol.* **9**, 255–265.

Sweeney, C., Gloor, E., Jacobson, A. R., Key, R. M., McKinley, G. and co-authors. 2007. Constraining global air-sea gas exchange for $CO_2$ with recent bomb C-14 measurements. *Global Biogeochem. Cycles* **21**, GB2015, doi:10.1029/2006GB002784.

Takahashi, T., Feely, R. A., Weiss, R. F., Wanninkhof, R. H., Chipman, D. W. and co-authors. 1997. Global air-sea flux of $CO_2$: an estimate based on measurements of sea-air pCO(2) difference. *Proc. Natl. Acad. Sci. USA* **94**, 8292–8299.

Takahashi, T., Sutherland, S. C., Wanninkhof, R., Sweeney, C., Feely, R. A. and co-authors. 2009. Climatological mean and decadal change in surface ocean $pCO_2$, and net sea-air $CO_2$ flux over the global oceans. *Deep-Sea Res. Part I-Oceanogr. Res. Papers* **56**, 2075–2076.

Tans, P. P. 1980. On calculating the transfer of C-13 in reservoir models of the carbon-cycle. *Tellus* **32**, 464–469.

Tans, P. P., Berry, J. A. and Keeling, R. F. 1993. Oceanic C-13/C-12 observations—a new window on ocean $CO_2$ uptake. *Global Biogeochem. Cycles* **7**, 353–368.

Thompson, M. V. and Randerson, J. T. 1999. Impulse response functions of terrestrial carbon cycle models: method and application. *Global Change Biol.* **5**, 371–394.

Thoning, K. W., Tans, P. P. and Komhyr, W. D. 1989. Atmospheric carbon-dioxide at Mauna Loa observatory, 2, analysis of the NOAA GMCC data, 1974–1985. *J. Geophys. Res.-Atmos.* **94**, 8549–8565.

Townsend, A. R., Asner, G. P., White, J. W. C. and Tans, P. P. 2002. Land use effects on atmospheric C-13 imply a sizable terrestrial $CO_2$ sink in tropical latitudes. *Geophys. Res. Lett.* **29**, 1426–1430.

Trolier, M., White, J. W. C., Tans, P. P., Masarie, K. A. and Gemery, P. A. 1996. Monitoring the isotopic composition of atmospheric $CO_2$: measurements from the NOAA Global Air Sampling Network. *J. Geophys. Res.-Atmos.* **101**, 25897–25916.

Van Der Werf, G. R., Randerson, J. T., Collatz, G. J., Giglio, L., Kasibhatla, P. S. and co-authors. 2004. Continental-scale partitioning of fire emissions during the 1997 to 2001 El Niño /La Nina period. *Science* **303**, 73–76.

Van Der Werf, G. R., Randerson, J. T., Giglio, L., Collatz, G. J., Kasibhatla, P. S. and co-authors. 2006. Interannual variability in global biomass burning emissions from 1997 to 2004. *Atmos. Chem. Phys.* **6**, 3423–3441.

Vaughn, B., Ferretti, D., Miller, J. and White, J. W. C. 2004. Stable isotope measurements of atmospheric $CO_2$ and $CH_4$. In: *Handbook of Stable Isotope Analytical Techniques* (ed. P. A. D., Groot). Elsevier, Amsterdam, London, 272–304.

Vaughn, B. H., Evans, C. U., White, J. W. C., Still, C. J., Masarie, K. A. and co-authors. 2009. Global network measurements of atmospheric trace gas isotopes. In: *Isoscapes, Understanding movement, pattern, and process on Earth through isotope mapping* (eds J. B., West, G. J., Bowen, T. E., Dawson and K. P., Tu). Springer, Amsterdam, 3–31.

Wanninkhof, R. 1992. Relationship between wind-speed and gas-exchange over the ocean. *J. Geophys. Res.-Oceans* **97**, 7373–7382.

Wetzel, P., Winguth, A., and Maier-Reimer, E. 2005. Sea-to-air $CO_2$ flux from 1948 to 2003: a model study. *Global Biogeochem. Cycles* **19**, GB2005, doi:10.1029/2004GB002339.

Winguth, A. M. E., Heimann, M., Kurz, K. D., Maierreimer, E., Mikolajewicz, U. and co-authors. 1994. El-Niño-Southern oscillation related fluctuations of the marine carbon-cycle. *Global Biogeochem. Cycles* **8**, 39–63.

Zhang, J., Quay, P. D. and Wilbur, D. O. 1995. Carbon-isotope fractionation during gas-water exchange and dissolution of $CO_2$. *Geochim. Cosmochim. Acta* **59**, 107–114.